CHAPTER 3

Schiff base derived multi-stimuli responsive conductive sonometallogel: a mechanistic insight into role of ultrasound in gelation

3.1 Introduction

We report here the synthesis of an ultrasound-induced multi-responsive fluorescent metallogel based on non-fluorescent citric acid derived ligand (1), LiOH and $Cd(OAc)_2$ in DMF. Ultrasound is shown to promote the de-metallation and recomplexation of Cd (II) ions proceeding through the disruption and reformation of dynamic metal-ligand coordination bonds, ultimately leading to gelation. Ultrasound also proved to be responsible for the formation of uniform nanofibers (~20 nm) characterized by AFM and TEM studies. The deviation from the aforesaid combination in terms of regioisomer, alkali base, and transition metal ion including Zn(II), solvent and triggering effect like mechanical or heat, could only produce solution instead of gel. The crystal structure obtained with Zn(II) analogous to metallogel constituents supports the structure involved in gelation with Cd(II). This "sonometallogel" is also found to be thermos-responsive and reversibly fluidized under suitable mechanical stress. The true gel phase material has been proved by a detailed rheological studies. Another key and yet unprecedented discovery is that the sonication-induced sol-gel phase transition leads to a tenfold increase in the conductivity values.

Gels are a unique class of responsive molecular materials [Li, Q. (Ed.). (2013)], Stuart *et al.* (2010), Cobo *et al.* (2015), Döring & Kuckling (2013), Zhuang *et al.* (2013), Ahn *et al.* (2008), Foster *et al.* (2010)]. A variety of additional properties such as conductance, optical, rheological, morphological, magnetic, catalytic, and/or redox can be incorporated into gels upon introducing metal ions to form metallogels [Whittell *et al.* (2011), Borré *et al.* (2016), Yan *et al.* (2012), Pandey *et al.* (2017), Tam & Yam (2013), Miao *et al.* (2013), Tu *et al.* (2011), Martínez-Calvo *et al.* (2015), Chen *et al.* (2015), Sutar & Maji (2016), Howlader & Mukherjee (2016), Gasnier *et al.* (2009), Steed (2010)]. Different

methodologies involving either chemical reactions, light irradiation, mechanical stress, or control of pH and temperature have been developed so far to produce gel materials [Naota, T., & Koori, H. (2005), Ghoussoub, A., & Lehn, J. M. (2005), van Herpt *et al.* (2013), Po *et al.* (2014)]. Sonication has also recently proved to be useful to produce metallogels and the ultrasound energy is thought to promote the rearrangement of molecules or specific conformational changes leading to spontaneous aggregation [Cravotto, G., & Cintas, P. (2009), Komiya *et al.* (2011), Isozaki *et al.* (2007), Sakong *et al.* (2012), Paulusse *et al.* (2007)]. Sonication has even been considered as being responsible for the demetallation and reorganization of coordinating units leading to gelation. In spite of all these fascinating results and of the most recent advances in gel chemistry, the design of a "sonometallogel", i.e., of ligand/metal mixtures capable of undergoing sonication induced metallogelation, is still a highly challenging task. Taking into account the above seminal findings and challenges, we now wish to report on the sonication induced formation of a fluorescent metallogel based on the highly selective combination of citric acid derived ligand, LiOH and $Cd(OAc)_2$ in DMF. We have established that the sonication process promotes a series of demetallation and re-metallation steps, ultimately leading to a transparent highly stable gel and also triggers the growth of well-defined and uniform nanofibers providing exceptional responsiveness and conducting properties to the metallogel. The present multi-responsive sonometallogel is thus not only unique as to its gelation mechanism but also in terms of the application opportunities opened up by its well-defined conductive nanostructure.

3.2 Instrumentation

Sonication experiment was performed on a Selec 1.5 L 50Hz/DTC (16.0 Watt, 33 ± 3 kHz) sonicator. Elemental analyses for carbon, hydrogen, and nitrogen were acquired on an Exeter CHN Analyzer CE-440. FT-IR and electronic absorption spectra were obtained on a PerkinElmer Spectrum 100 and Thermo scientific EVOLUTION 201 spectrophotometers, respectively. Photoluminescence spectra were acquired on a Perkin Elmer LS 55 spectrophotometer. The lifetime measurements were made using a TCSPC system from Horiba Yovin (Model: Fluorocube-01-NL). The samples were excited at 378 nm using a picosecond diode laser (Model: Pico Brite-375L) and data analysis was performed using IBH DAS (version 6, HORIBA Scientific, Edison, NJ) decay analysis software. ^{1}H NMR spectra were obtained on a Bruker AVANCE III HD 500 spectrometer. Electrospray ionization mass (ESI-MS) spectra were recorded on a Waters (Micromass MS Technologies) QTof Premier. Thermal Gravimetric analysis data was acquired on a NETZSCH STA 449 F3 at a heating rate of 5 °C min^{-1} under a nitrogen atmosphere. TEM images and AFM were captured using a JEOL JEM 2100 and NT-MDT NTEGRA PRIMA, respectively. Powder XRD data were collected on Rigaku MiniFlex 600 Detector D-tex ultra between angle 2θ = 5-80°.

Solution electrical conductivity was measured on a Eutech Instruments CON 5/TDS 5 Conductivity Meter. The instrument was calibrated with the standard solution. The rheology of sonometallogel was performed on Anton Paar MCR 702 Twin Drive Rheometer. Impedance measurements have been carried out with a Biologic® ESP 300 potentiostat equipped with a built-in computer-controlled Frequency Response Analyzer (FRA).

3.2.1 Calibration of ultrasonic bath

Low power continuous ultrasonic waves irradiated for gelation at a constant frequency of 33 kHz. The power of ultrasonic waves was calibrated using a standard calibration procedure. A known volume of water (20 mL) taken in a reaction vessel and it is subjected to ultrasonic irradiation for a known time. A graph between time and temperature plotted and with the help of slope of the time-temperature plot, power of ultrasonic source was determined using the following equations

$$dQ = m.cp.dT$$

Where c_p is heat capacity of water (4.2 J/g)

OR

$$dQ/dt = m.c_p.dT/dt$$

OR

$$Power = m.c_p.dT/dt$$

Thus, the acoustic power of the ultrasonic bath calculated and found to be 16.0 Watt for a water sample.

Note: Calibration of ultrasonic bath repeated in triplicate for water samples fixed in the middle of the bath.

3.2.2 Rheological Study

Measurements were performed using a stress-controlled rheometer (Anton Paar MCR 702 TwinDrive) equipped with stainless steel parallel plates (20 mm diameter, 0.5 mm gap). Experiments were carried out on freshly prepared gels (0.6 % w/v). Linear viscoelastic regions of the samples were determined by measuring the storage modulus, G' (associated with energy storage), and the loss modulus G" (associated with the loss of energy) as a function of the stress amplitude. Dynamic oscillatory work was kept at a frequency of 0.01 rad s^{-1}. The following tests were performed: increasing amplitude of oscillation up to 100% apparent strain on shear, time and frequency sweep at 25 °C (~28 min and from 0.01 to 100 rad s^{-1}, respectively), and heating run to 160 °C at a scan rate of 5 °C min^{-1}. All these measurements were conducted in duplicate.

3.2.3 Conductance Study

Impedance measurements have been carried out with a Biologic® ESP 300 potentiostat equipped with a built-in computer controlled Frequency Response Analyzer (FRA) operating over a frequency range of 10 μHz up to 7 MHz. Home-made one-compartment, two-electrode cells allowing to position two identical cofacially oriented stainless steel or platinum electrodes at a fixed distance has been used to estimate the conductivity of each sample. Variable temperature measurement of the conductivity has been carried out in a home-made jacketed glass cell incorporating two platinum electrodes (Ø = 1cm). The temperature in the cell was controlled with a Lauda-Brinkman RE 104 thermostat. Electrical impedance measurements have been performed in a potentiostatic regime at E_oC between 1Hz and 2.5MHz using a maximum voltage of 0.01V. Fitting the experimental

Nyquist impedance diagrams (–Im(Z) vs. Re(Z)) was achieved with Z-fit using equivalent electrical circuits involving the actual resistance of the sample R1, a capacitance C1 and a constant-phase element Q1.

Such fitting allowed to estimate the resistance of each sample corresponding to the intersection of the curve with the real part of the impedance. The conductivity was calculated from the electrolyte resistance (R_1) using the equation:

$$\sigma = l / R\kappa \quad (1)$$

Where κ is the conductivity in $S.m^{-1}$, R is the ohmic resistance of the electrolyte, l is the distance between the two electrodes (m), and S is the area of the electrodes (m^2). The cell constant, (l /S) was determined at 25°C by calibration with standard 0.01D and 0.1D KCl solutions having known conductivity values, (1408 μS.m-1, 1285 $mS.m^{-1,}$ and 11.13 $S.m^{-1}$).

3.3 Synthesis of Intermediate and Isomers 1 & 2

3.3.1 Synthesis of CAHN

The precursor compound citric hydrazone was synthesized by mixing the triethyl citrate (0.200 g, 0.74 mmol) and hydrazine hydrate (0.150 g, 2.97 mmol) in methanol (20 mL) at constant stirring for 20 min. The resulting solution was refluxed for an additional 6 hours. Upon cooling to room temperature, it afforded a white crystalline powder which was isolated by filtration, washed with diethyl ether and dried in vacuum desiccators. Yield 0.145 g (85%). IR (KBr): $\upsilon(NH_2)_{sym}$ 3357, $\upsilon(NH)_{sym}$ 3292, υ(C=O) 1662 (s).

3.3.2 Synthesis of Isomer 1

The precursor compound CAHN (0.200 g, 0.85 mmol) was dissolved in 2 mL water and then mixed with 20 mL methanol to obtain a clear solution. Methanolic solution (5 mL) of 2-hydroxybenzaldehyde (0.313 g, 2.56 mmol) was added dropwise to CAHN solution and the resulting solution stirred for an additional 3 hours. It afforded a white precipitate, which was filtered, thoroughly washed with chloroform, methanol and Hexane and dried under vacuum. Yield 0.345 g (74%). Anal. Calcd. for $C_{27}H_{26}N_6O_7$: C, 59.32; H, 4.79; N, 15.38. Found C, 59.14; H, 4.86; N, 15.09. m/z (ESI- MS, $[1+H]^+$), 547.19 (calcd. 547.19). To obtain the single conformer, ^{1}H NMR measurement was performed by dissolving the solid in [D_6] DMSO in the presence of 3 Equiv. of LiOH•H_2O. UV-vis. [DMF, λ_{max}, nm (ε, M^{-1} cm^{-1})]: 322 (40000), coupled 292, 281 (59000).

3.3.3 Synthesis of Isomer 2

It was synthesized following the similar procedure described for 1, using 4-hydroxybenzaldehyde instead of 2-hydroxybenzaldehyde. Yield 0.330 g (71%). Anal. Calcd. for $C_{27}H_{26}N_6O_7$: C, 59.32; H, 4.79; N, 15.38. Found C, 59.26; H, 4.64; N, 15.21. m/z (ESI-MS, $[1+H]^+$), 547.19 (calcd. 547.19). IR (KBr, cm^{-1}): υ(–NH) 3247, υ(C=O) 1661- 1606 (s), υ(C=N) 1513 (s). UV-vis. [DMF, λ_{max}, nm (ε, M^{-1} cm^{-1})]: 310 (58500), 295 (70500).

3.3.4 Synthesis of 1/Li^+/Cd(II) (non-sonicated) complex

Isomer 1 (5.0 mg, 9 mmol) was dissolved in DMF (0.6 mL) in a vial followed by the deprotonation with LiOH•H_2O (1.15 mg, 27 mmol) resulted in a pale yellow color clear solution. The freshly prepared $Cd(OAc)_2$ (3.66 mg, 13 mmol) solution in DMF (0.4 mL) was added to the deprotonated solution of 1 and the resulting transparent clear yellow color mixture solution left for stirring for 5 hours. The resulting solution was evaporated under reduced pressure to complete dry. The ensuing solid was washed with excess water, methanol and diethyl ether to remove salts and other impurity formed during the course of the reaction. Yield 74%. Anal. Calcd. for: $[LiCd(C_{27}H_{23}N_6O_7)].13H_2O$: C, 36.07; H, 5.49; N, 9.35. Found C, 36.06; H, 5.45; N, 9.41. ESI−MS m/z: $[Cd(C_{27}H_{25}N_6O_7)]^+$, 659.08 (calcd. 658.08). IR (KBr, cm^{-1}) υ(C=O) 1659, 1612, 1546; υ(C=N) 1468.

3.3.5 Synthesis of 1/Li^+/Zn(II) complex

To a methanolic suspension of isomer 1 (0.100 g, 0.183 mmol), LiOH was added (0.023 g, 0.549 mmol) at constant stirring which led to a clear solution. The methanolic solution of $Zn(OAc)_2$ (0.060 g, 0.274 mmol) was added to the above stirring mixture which immediately produced the pale yellow precipitate. Further, this solution was filtered after 6 hours stirring at room temperature and the residue was recrystallized by the DMF-water layering method. Light yellow colored green fluorescent crystals were obtained within ten days. Yield ~45%. Anal. Calcd. for: $[Zn_3(C_{27}H_{23}N_6O_7)_2].12H_2O$: C, 43.36; H, 4.72; N, 11.24. Found C, 43.23; H, 4.68; N, 11.54. ESI−MS m/z: $[Zn_3(C_{27}H_{22}N_6O_7)_2H]^-$, 1281.09 (calcd. 1281.10). IR (KBr, cm^{-1}) υ(C=O) 1643, 1614, 1538; υ(C=N) 1468. Weight loss as per TGA: 15.66 % (calcd. for: $13H_2O + CH_3OH$ 15.63%).

Note: Use of KOH and $Zn(ClO_4)_2$ or filtrate or DMF also produce similar crystal with equal crystallographic parameter.

3.3.6 Synthesis of metallogel (C2)

Isomer 1 (5.0 mg, 9 mmol) was dissolved in DMF (0.6 mL) in a vial followed by the deprotonation with $LiOH•H_2O$ (1.15 mg, 27 mmol) resulted in a pale yellow colour clear solution. The freshly prepared $Cd(OAc)_2$ (3.66 mg, 13 mmol) solution in DMF (0.4 mL) was added to the deprotonated solution of 1 and the resulting transparent clear yellow colour mixture solution sonicated for 2 minutes. The sonicated mixture thus obtained was left undisturbed for 2 minutes to achieve the transparent and stiff gel, which was tested by a conventional inverted vial method.

The resulting gel was dried under vacuum and washed with water to remove additional salt formed during the course of the reaction. The isolated vacuum dried compound used for further data analysis. Anal. Calcd. for $[LiCd(C_{27}H_{23}N_6O_7)].6H_2O$: C, 41.96; H, 4.56; N, 10.88. Found C, 41.78; H, 4.63; N, 10.84. ESI−MS (diluted gel) m/z: $[(C_{27}H_{25}N_6O_7)Cd]^+$, 659.08 (calcd. 659.08). IR (KBr, cm^{-1}): υ(C=O) 1661, 1610, 1539 (s), υ(C=N) 1470 (m). Weight loss as per TGA: 5.39 % (calcd. for $2H_2O$ 5.47 %); 10.85 % (calc. for DMF 11.09 %) and 14.06, 13.75, 22.88 % are corresponding to various kind of degradation of ligand. Molar conductance of isolated compound (xerogel washed with water to remove extra salt formed during the course of reaction and vacuum dried) found to be 15 ohm^{-1} cm^2 mol^{-1} in DMF which indicates the nonconductive nature of the isolated complex.

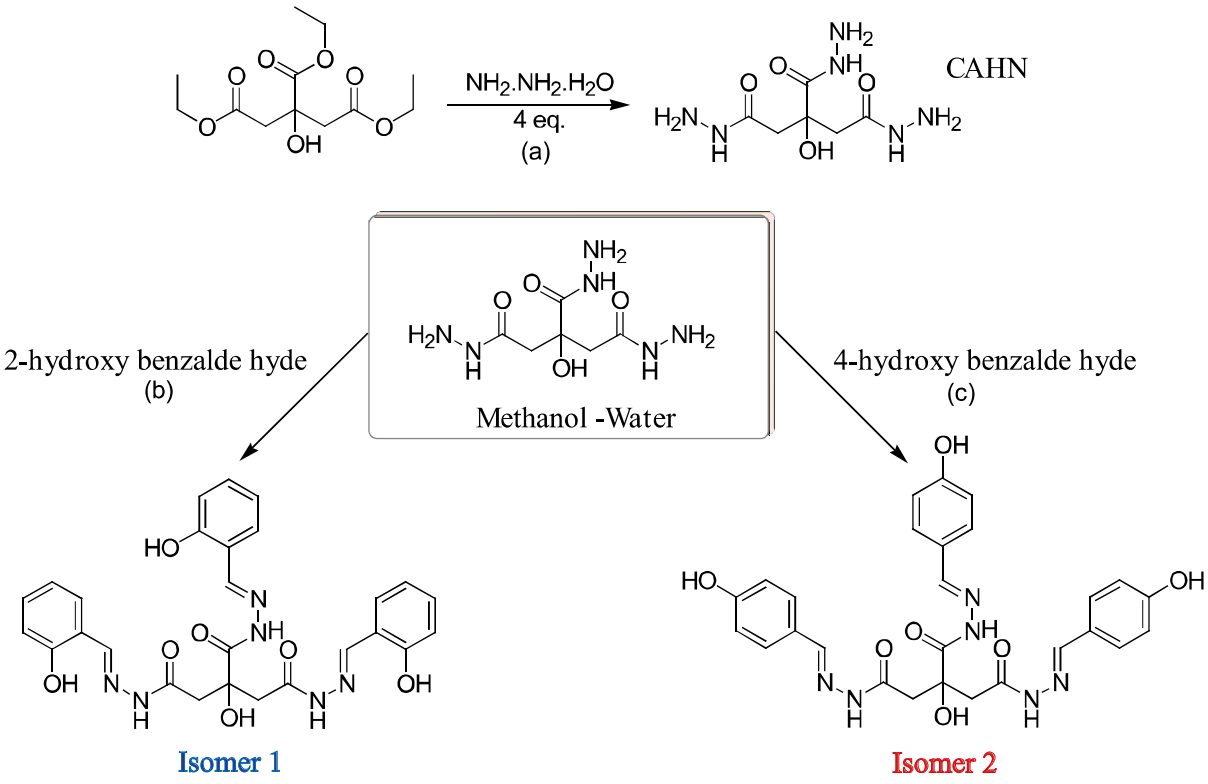

Scheme 3.1 Synthetic Strategy adopted for Isomer 1 & 2 via Schiff base reaction method

3.4 Result and discussion

The synthesized isomer 1 and 2 were characterized by various instrumental methods such as ^{1}H NMR and Mass Spectrometry.

3.4.1 NMR Characterization

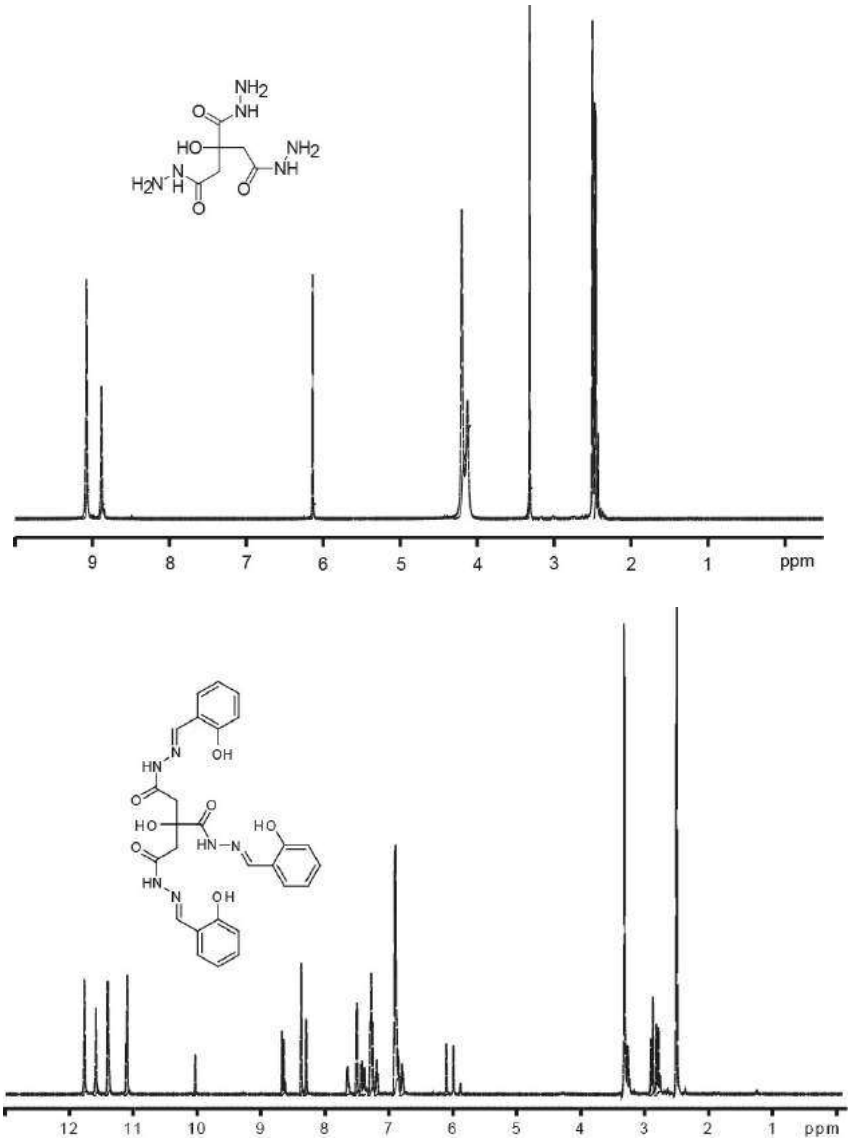

Figure 3.1 ^{1}H NMR spectra (500 MHz, DMSO-d6, 298 K) for (A) precursor compound citric hydrazine (CAHN), (B) isomer 1, where sketch diagram of two plausible conformers anti-anti-syn and syn-anti-syn in the ratio of 3:2 are pasted along with their corresponding asterisk and oval shape symbol label and (C) two plausible conformers anti-anti-syn and syn-anti-syn of isomer 1 converted into single conformer anti-anti-anti upon treatment with LiOH. The labile protons regions –NH and –OH were deprotonated after treatment with LiOH (deprotonated region shown by blue dotted circle)

CAHN ^{1}H-NMR (500 MHz, [D_6] DMSO, 25 °C): δ = 9.08 (s, 2 H); 8.88 (s, 1 H); 6.14 (s, 1 H); 4.16 (d, 6 H); 2.47-2.42 (m, 4 H).

Isomer 1 ^{1}H-NMR (500 MHz, [D_6] DMSO, 25°C): δ = 8.48 (s, 1 H, =CH); 8.20 (s, 2 H, =CH); 7.26- 7.10 (m, 6 H, Ar); 6.76- 6.66 (m, 6 H, Ar); 2.69, 2.58 (dd, 4 H, -CH_2).

Isomer 2 ^{1}H-NMR (500 MHz, [D_6] DMSO): δ =8.29(s, 1 H, =CH); 8.04 (s, 1 H, =CH); 7.87 (s, 1 H, =CH); 7.43 (s, 6 H, Ar); 6.74 (s, 6 H, Ar); 2.70 (d, 4 H, -CH_2).

3.4.2 ESI Mass Characterization

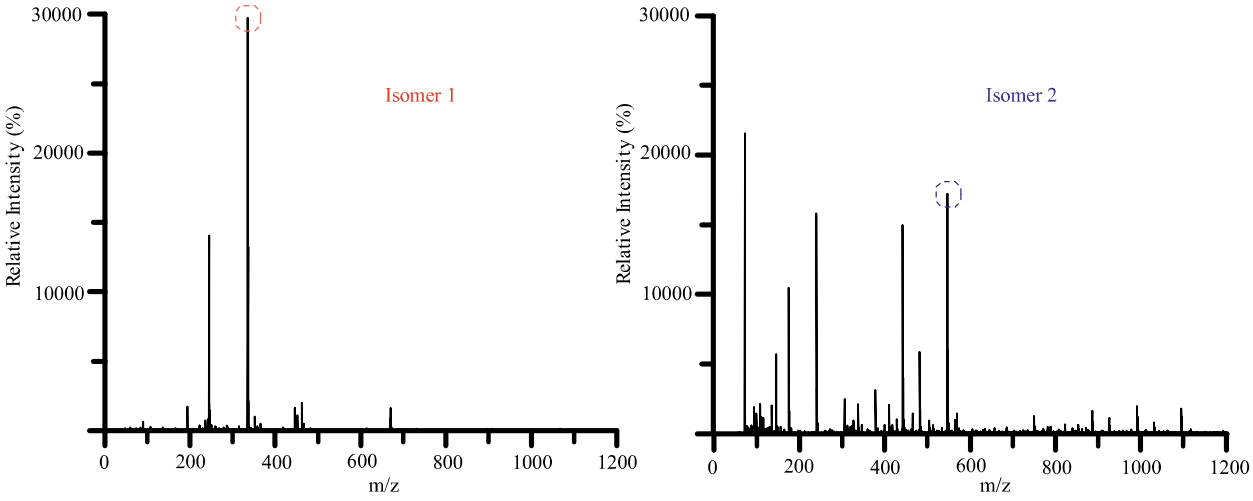

Figure 3.2 ESI-MS spectra of Isomer 1 and isomer 2

3.4.3 Studies on Conformational isomers

Syn and Anti conformation notations: The citric acid-based isomer 1 has three arms for metal binding, and each arm has its own orientation in space. Let's consider one arm of ligand 1- If the phenolic –OH and -C=O are lying in the same direction then the notation will be syn. If both the –OH and -C=O prefer to stay in the opposite direction to each other, than the conformation will be anti. Thus, we assigned these notations for the entire three arms for instance, anti/anti/syn. For further detail, see- B. Levranda, W. Fiebera, J. M. Lehn, and A. Herrmann, Helv. Chim. Acta, 2007, 90, 2281.

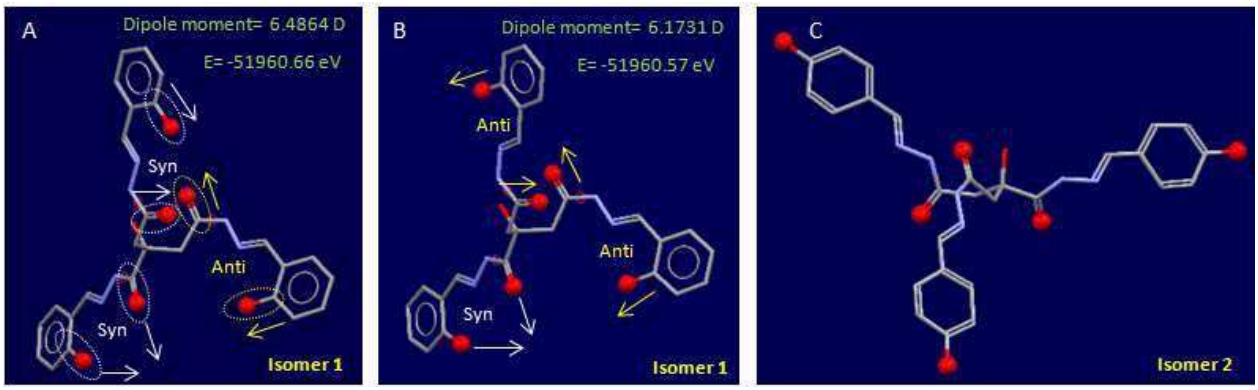

Figure 3.3 DFT optimized structures of (A) Syn-Syn-Anti and (B) Anti-Anti-Syn conformers of isomer 1 with their dipole moments and energies, respectively

^{1}H NMR well demonstrates these two conformers in 2:3 ratio and (C) model of corresponding regioisomer 2 with no conformer possibilities which was also observed experimentally in ^{1}H NMR (vide infra) [Levrand *et al.* (2007), Ranford *et al.* (1998)]. DFT structural optimization of these two conformers shows that the significant dipole moment and minor energy difference (anti/anti/syn E= -51690.5763, dipole moment= 6.1731; anti/syn/syn E=-51690.6608 eV, dipole moment= 6.4864) support the result obtained from ^{1}H NMR.(Figure 3.3)

Gelation Combination

Table 3.1 Gelation ability of Isomer 1 with various bases and metal salts

Metal salt	LiOH	NaOH	KOH	CsOH
$Zn(OAc)_2 \cdot 2H_2O$	S	S	S	S
$Cu(OAc)_2 \cdot H_2O$	SP	SP	SP	SP
$Ni(OAc)_2 \cdot 4H_2O$	S	S	S	S
$Co(OAc)2 \cdot 4H_2O$	S	S	S	S
$Mn(OAc)_2.H_2O$	S	S	S	S
$Cd(OAc)_2 \cdot 2H_2O$	**G**	S	S	S
$Cd(NO_3)_2.6H_2O$	S	S	S	S
$CdCl_2$	S	S	S	S
$Zn(NO3)_2.6H_2O$	S	S	S	S
$Zn(ClO4)_2.6H_2O$	S	S	S	S

Table 3.2 Solubility of Isomer with various solvents

Solvent	Solubility/Gelation ability
DMSO	SP
Methanol	SP
Ethanol	SP
Water	SP
Acetone	I
Acetonitrile	I
Ethyl Acetate	I
DCM	I
THF	I
Chloroform	I
1,4-Dioxane	I
Hexane	I

Table 3.3 The characterization data for 1/Zn(II) crystal and 1/Cd(II) gel tabulated for comparison which clearly indicates the two different structures in Zn(II) crystal and Cd(II) gel

S.N.	Experiment	1/Zn(II) (crystal)	1/Cd(II) (xerogel)
1.	IR (cm^{-1})	υ(C=O) 1643, 1614, 1538, υ(C=N) 1468.	υ(C=O) 1661, 1610, 1539,υ(C=O) 1470.
2.	UV-vis (nm)	376	378
3.	Job's plot (M:L)	3:2	1:1
4.	ESI-Mass (*m/z*)	1281.09	659.08
5.	Conductance ($ohm^{-1}cm^2mol^{-1}$, DMF)	12	15
6.	CHN analysis	$Zn_3(C_{27}H_{23}N_6O_7)_2].12H_2O$: Calcd. C, 43.36; H, 4.72; N, 11.24. Found C, 43.23; H, 4.68; N, 11.54.	$[LiCd(C_{27}H_{23}N_6O_7)].6H_2O$: Calcd. C, 41.96; H, 4.56; N, 10.88. Found C, 41.78; H, 4.63; N, 10.84.
7.	Weight loss as per TGA:	15.66% (calcd. $13H_2O+CH_3OH$ 15.63%) remaining two-step degradation corresponding to ligand	5.39% (calcd. for $2H_2O$ 5.47%); 10.85 % (calcd. for DMF 11.09%) and 14.06, 13.75, 22.88% are corresponding to various kind of degradation of ligand
8.	Fluorescence spectra (nm)	470	468
9.	Effect of ultrasonication		
10.	a) UV-vis spectra	No change	Demetallation & Remetallation observed
11.	b) Fluorescence spectra	No change	Demetallation & Remetallation observed
12.	Molecular formula	$[(C_{27}H_{23}N_6O_7)_2Zn_3]$	$[C_{27}H_{24}N_6O_7Cd]$
13.	Nature of molecule	Trinuclear complex	Coordination polymer

Investigations carried out with various solvents, alkali bases (NaOH, KOH, CsOH) and Cd(II) salts led us to the conclusion that the gelation process is highly selective as it specifically requires the presence of DMF, LiOH and $Cd(OAc)_2$.

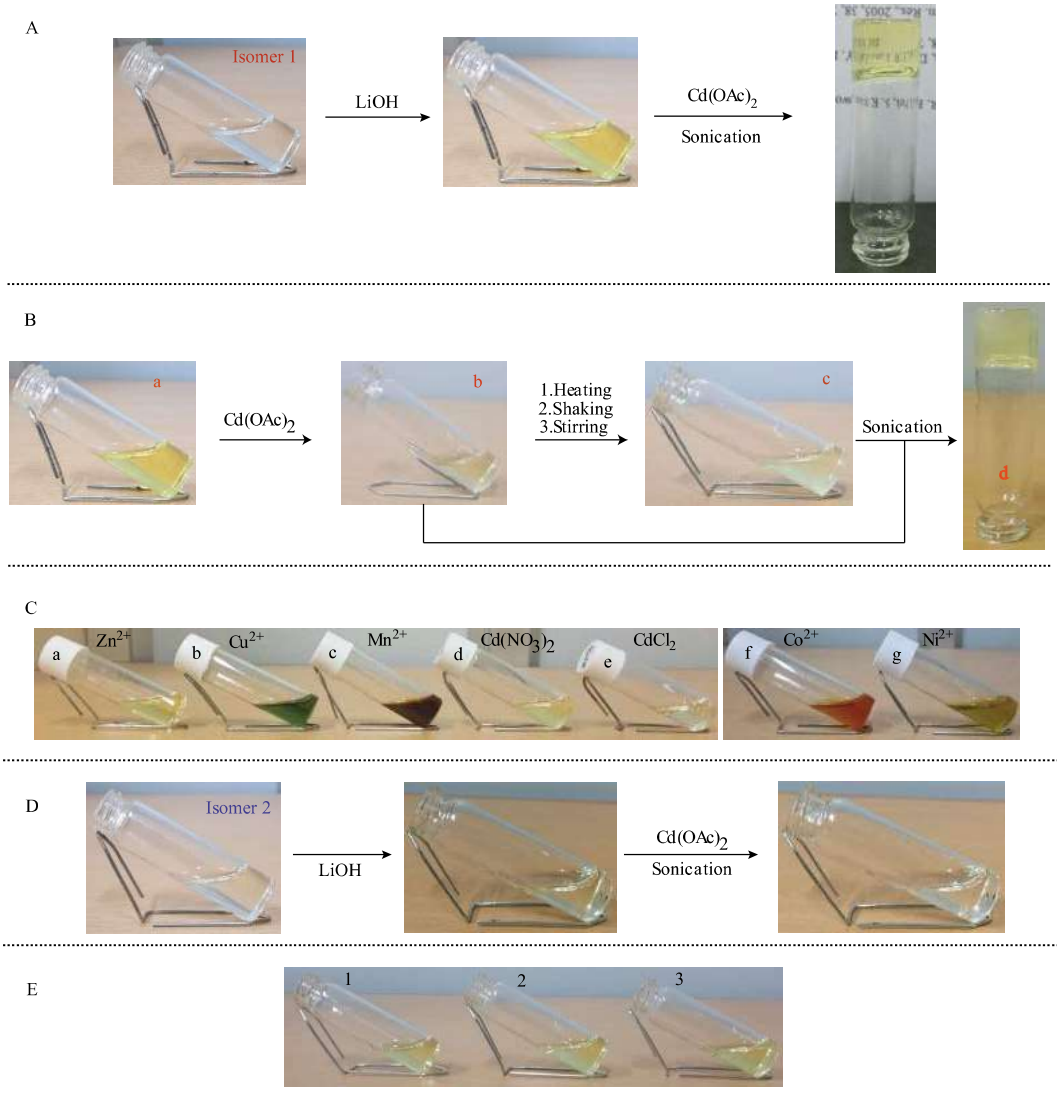

Figure 3.4 (A) Absence of gelation with other metal salts a) $Zn(OAc)_2$, b) $Cu(OAc)_2$, c) $Mn(OAc)_2$, d) $Cd(NO_3)_2$, e) $CdCl_2$, f) $Co(OAc)_2$, g) $Ni(OAc)_2$, (B) Gelation test of isomer 2+LiOH with $Cd(OAc)_2$ in DMF under similar conditions to isomer 1 shows transparent solution instead of gel indicating the importance of position of –OH in gelation. (C) Isomer 1 with NaOH, KOH, CsOH (a, b and c respectively) possess similar visible appearance as isomer 1+ LiOH but show no gelation with $Cd(OAc)_2$ under similar conditions

3.4.4 Schematic representation of formation of gel step by step

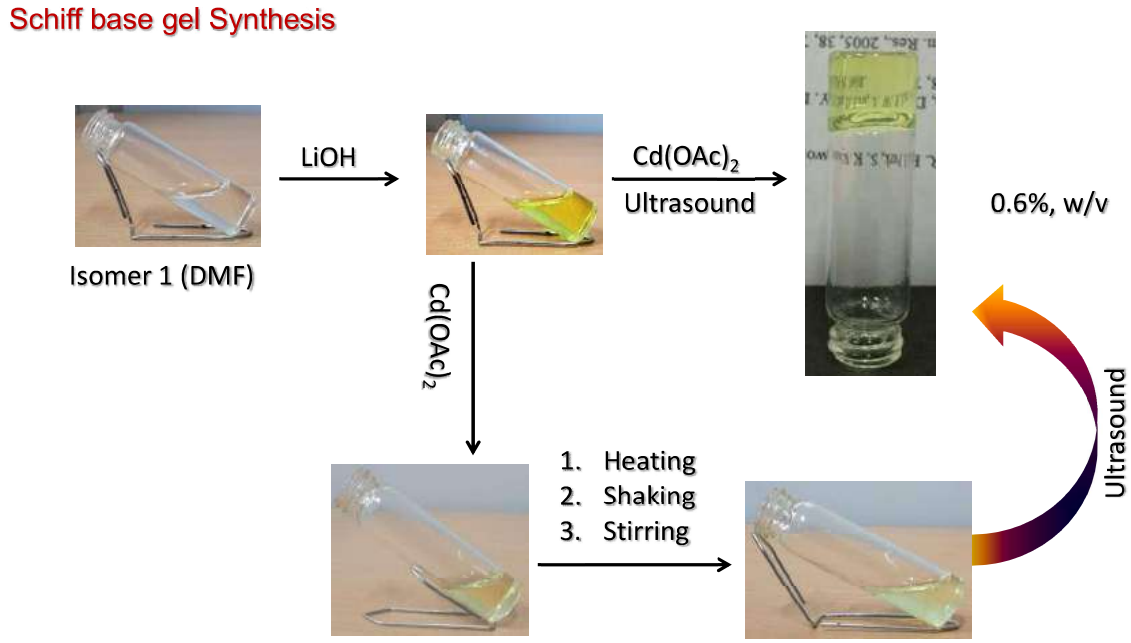

Gelation is highly selective towards isomer 1, LiOH, $Cd(OAC)_2$ and DMF under sonication.
Transparent enough to read the object

Figure 3.5 Mode and the role of various physical stimuli upon gelation behavior has been observed

3.4.5 Physical properties of metallogel

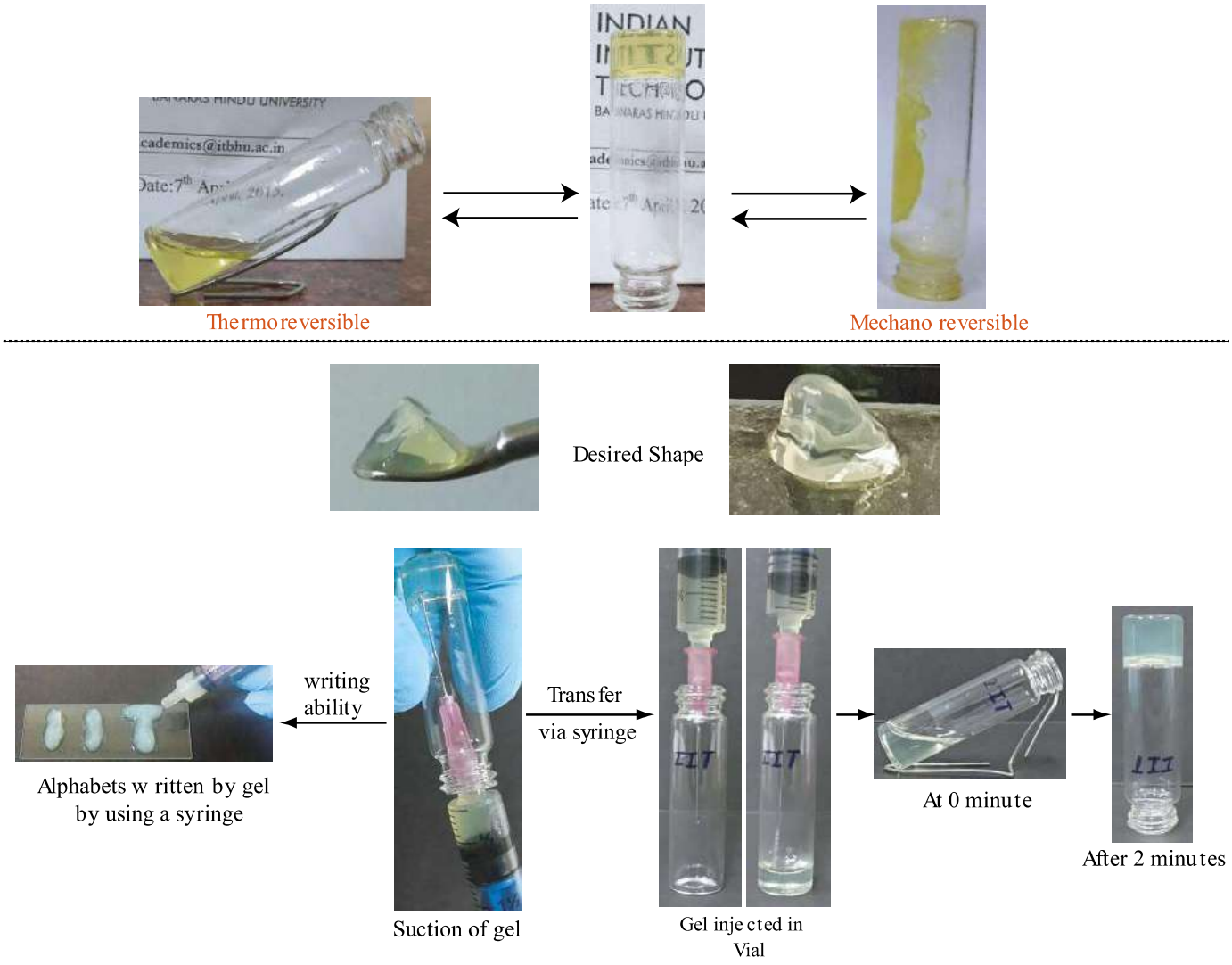

Figure 3.6 A pictorial representation among various manners of physical assets in one gel ('many in one') like (A). Thermal as well as mechanical reversible property, (B) can be utilized for writing purpose and also can be transferred through injection from one vial to another vial

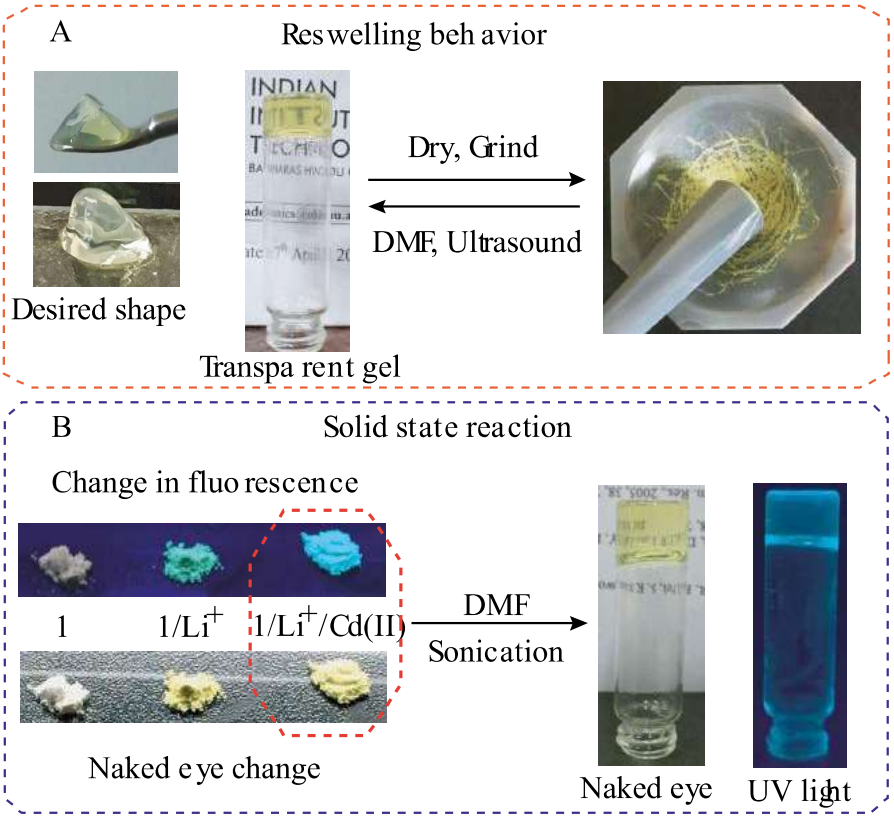

Figure 3.7 Solid-state reaction of isomer 1 with LiOH upon grinding produced fluorescence (light green), and upon further addition of Cd(II), it produces blue fluorescence. Interesting to note that upon the addition of DMF and after sonication, this solid pre-gelator performed gelation again

3.4.6 Change in gelation behavior of Isomer 1 and 2

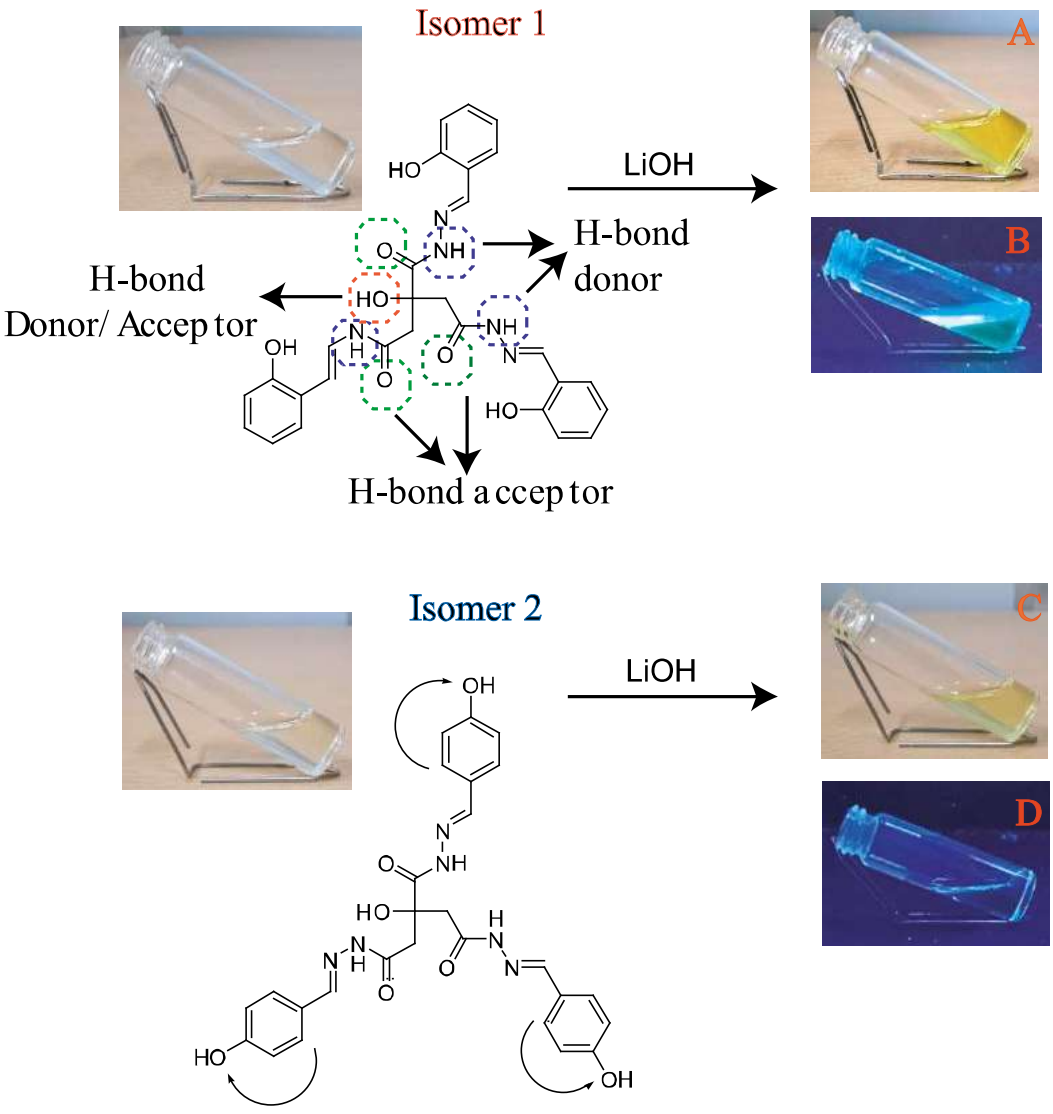

Figure 3.8 Change in behavior of gelation for isomer 1 and 2 were observed along with binding moieties responsible for gel formation

The morphology of the diluted metallogel ($1x10^{-5}$ M) was further acquired by TEM and AFM. Both TEM and AFM images recorded after sonication revealed the presence of three-dimensional (3-D) networks involving thin nanofibers of about ~20 nm in diameter and of several micrometers in length.(Figure 3.9) These well-defined structures stand in sharp contrast to the wrecked non-directional aggregates observed in the same conditions before sonication, which clearly brings to light the key role of sonication in the structuring process associated with gelation [Yu *et al.* (2014), Bardelang *et al.* (2008)].

3.4.7 TEM Images before and After Sonication

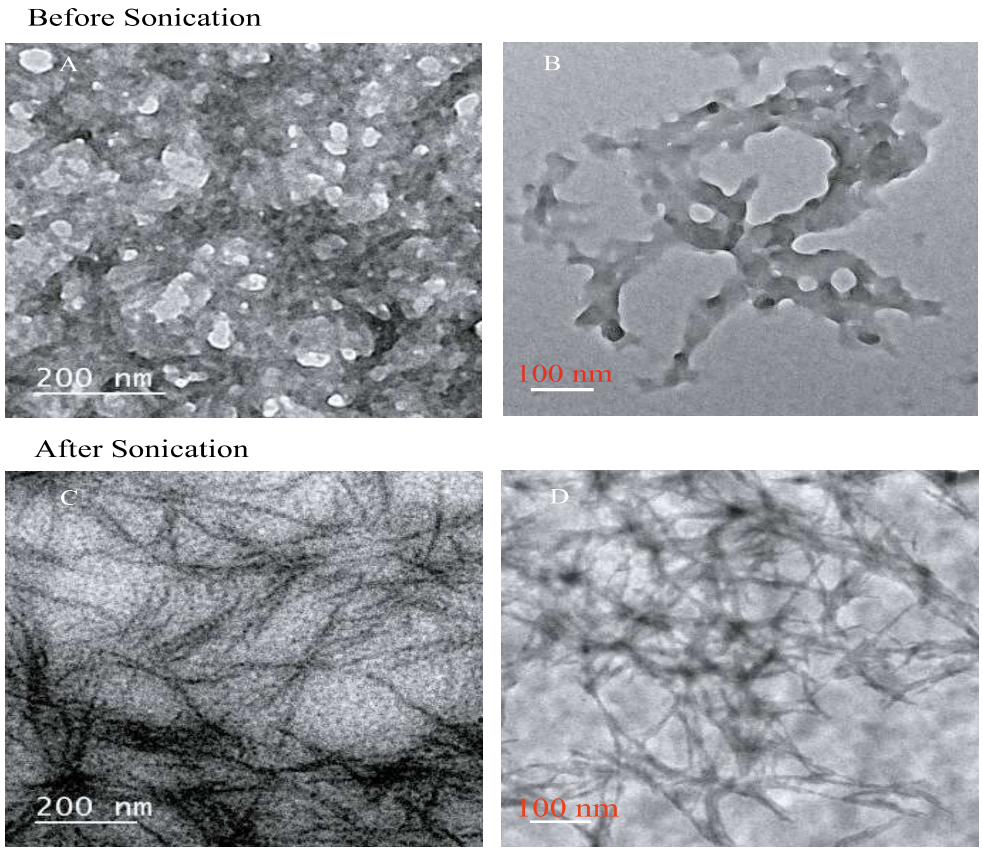

Figure 3.9 TEM images of diluted samples ($1x10^{-5}$ M) (A, B) before sonication reveals non directional wrecked aggregate growth at two different magnifications and (C, D) upon sonication wrecked aggregate converted into well ordered, directional, long-range nano-fibers with average diameter of ~20 nm

3.4.7.1 Change in morphology upon sonication (visible through TEM)

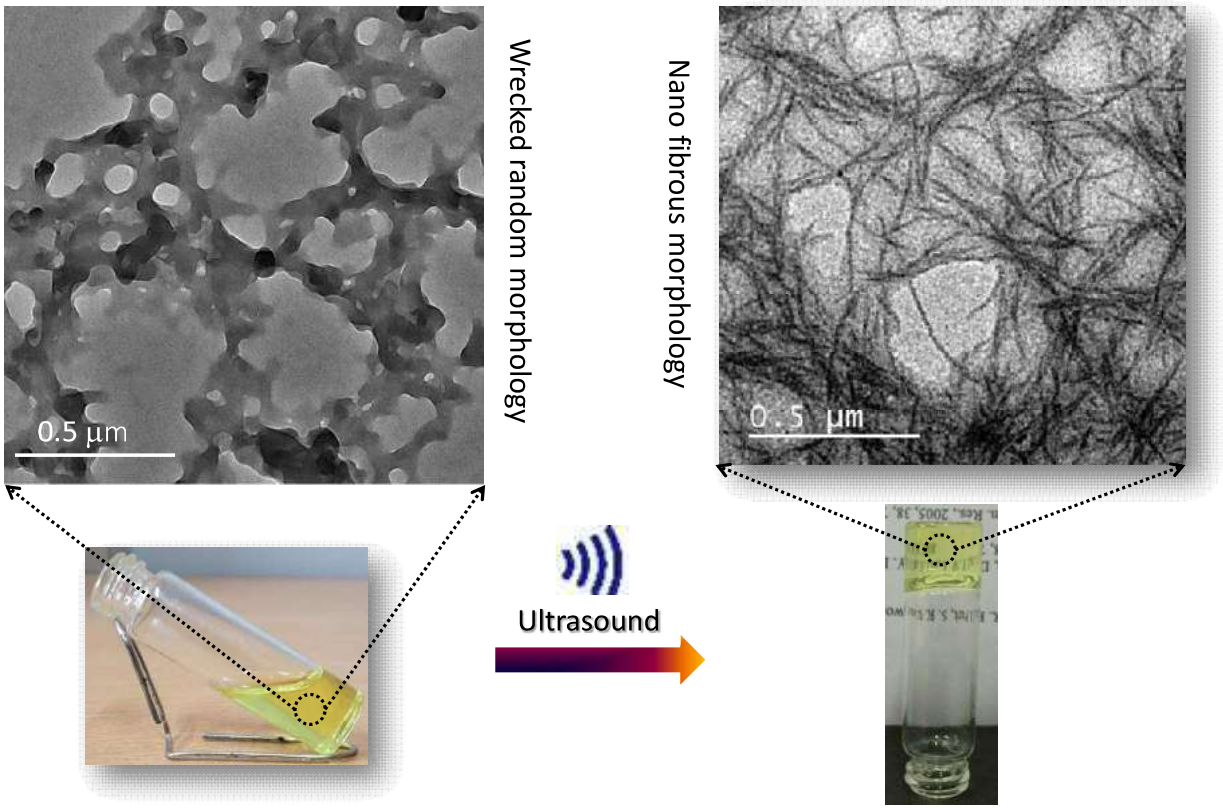

Figure 3.10 TEM images of non-sonicated solution and TEM images captured after sonication

3.4.8 Atomic Force Microscopy

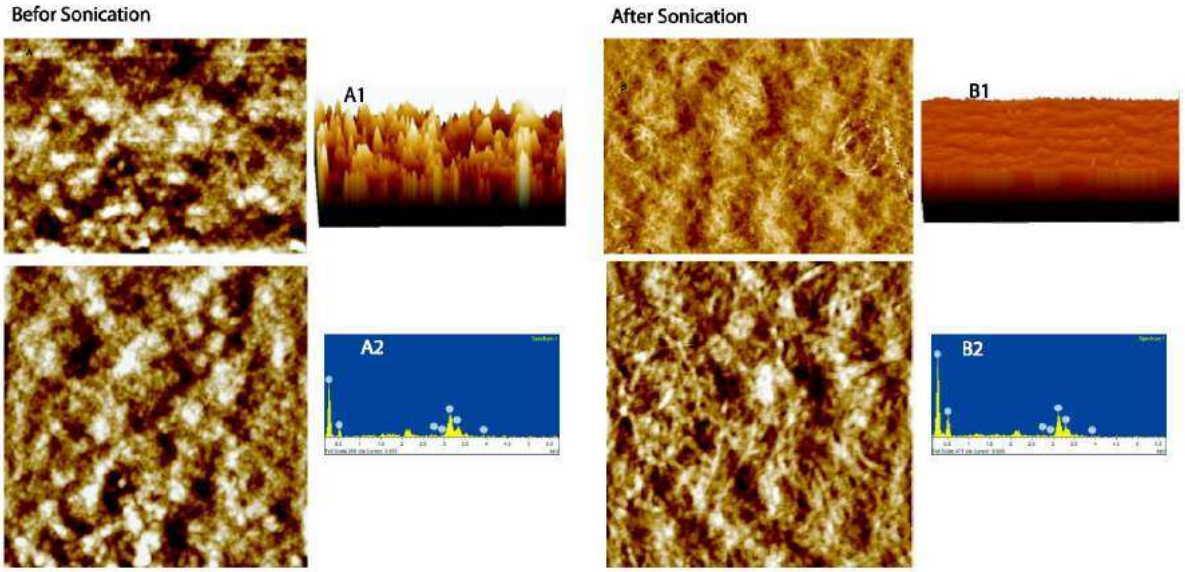

Figure 3.11 AFM images of diluted samples ($1x10^{-5}$ M) (A) Before Sonicated, sample exhibiting scattered aggregate appearance with (A1) rough surface morphology, and (B) Sonicated diluted gel, showing nano-fibrous morphology with (B1) almost smooth surface structure appeared due to the uniform nanofiber formation. (A2, B2) EDAX plot shows that the elemental profile is quite similar before and after sonication

3.4.9 UV-visible spectroscopy of Isomer 1 with various metals

Electronic absorption study has been undertaken in order to investigate the complexation process as well as to get further insights into the role of sonication. Isomer 1 ($1x10^{-5}$ M, DMF, 298 K) displays two intense coupled absorption bands at 281 and 291 nm attributed to π–π* transition, as well as a less intense band centered at 322 nm, ascribed to a n-π* transition [Wang *et al.* (2011)]. There was no significant change observed upon deprotonation of 1 with LiOH (3 equiv.), whereas aliquot addition of $Cd(OAc)_2$ ($1.0 x10^{-3}$ M, DMF) to a deprotonated solution of 1 led to the progressive disappearance of the band centered at 322 nm at the expense of a new signal growing at 378 nm through nice isosbestic point at 342 nm. Such spectral changes suggest the transformation of the deprotonated ligand into a coordination complex. Ratiometric change with a bathochromic shift of 55 nm also signifies conformational changes in 1 under the influence of binding of Cd(II) during the complexation [Isla *et al.* (2016), Ihara *et al.* (2015)]. The changes observed on the UV-vis absorption spectrum when submitting a 1/LiOH/$Cd(OAc)_2$ mixture (1:3:1) to sonication. One key feature of the observed sonication-induced modifications, proceeding through the same isosbestic point at 342 nm, is the gradual disappearance of the main band centered at 378 nm, attributed to the initial Cd(II) complex, at the expense of new bands at λ_{max} = 281, 291 and 322 nm, fully matching those of the free ligand 1 (figure 3.16).

We have also discovered that another set of changes appears once sonication stops, leading, within 5 minutes of resting, to a complete recovery of the initial signature attributed to the Cd(II) complex. The overall results discussed above under sonication and resting conditions thus support the conclusion that sonication of a 1/3/1 mixture of 1/LiOH/Cd(II) in

DMF promotes the dissociation of the initial complex formed upon mixing, and that this solution evolves upon resting towards new Cd(II) adducts featuring gelation abilities. It is worth mentioning that such demetallation/remetallation processes have not been observed from mixtures of 1/LiOH/$Zn(OAc)_2$ or 1/KOH/$Cd(OAc)_2$ in DMF. Similar investigations carried out with isomer 2 also support the conclusion that neither the complexation with Cd(II) nor the gelation takes place with the para phenol isomer (figure 3.12-3.18).

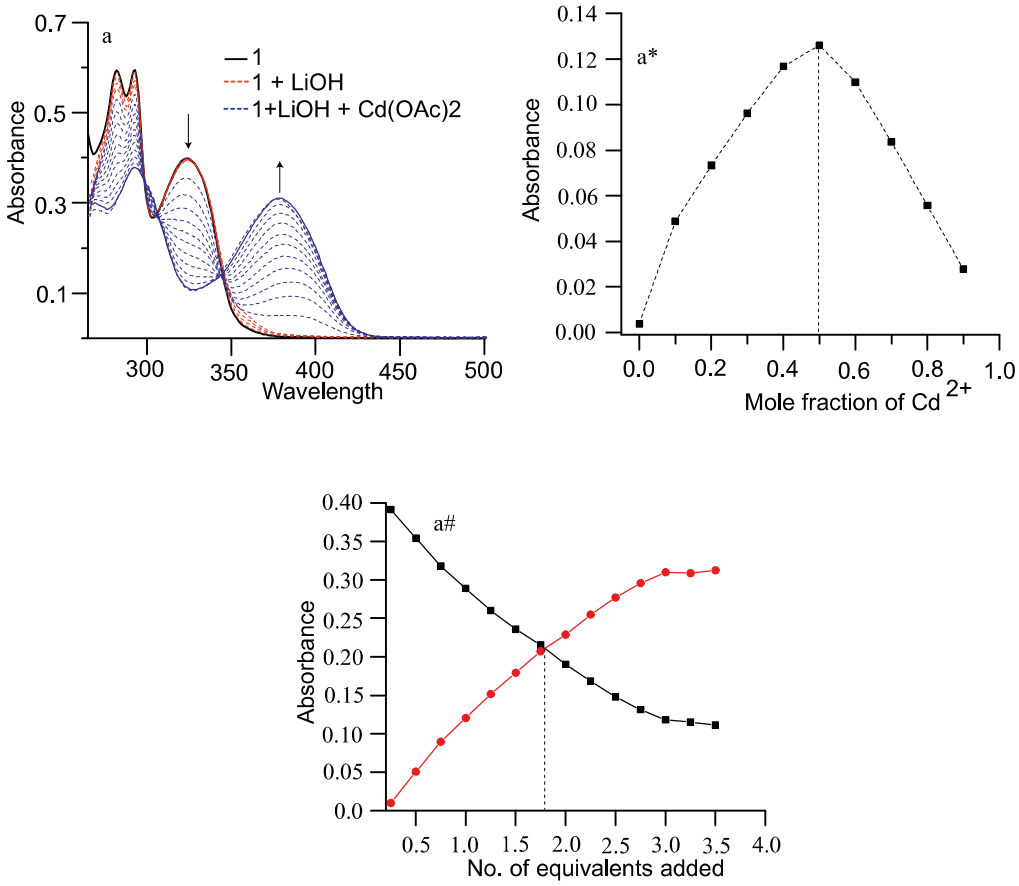

Figure 3.12 (a) UV-vis titration of Isomer 1 with $Cd(OAc)_2$ in the presence of LiOH as base showing the isosbestic change in spectra in a regular manner (a*) Job's Plot data of $Cd(OAc)_2$ with Isomer 1 ($a^{\#}$) Number of equivalents added till last aliquot of metal addition

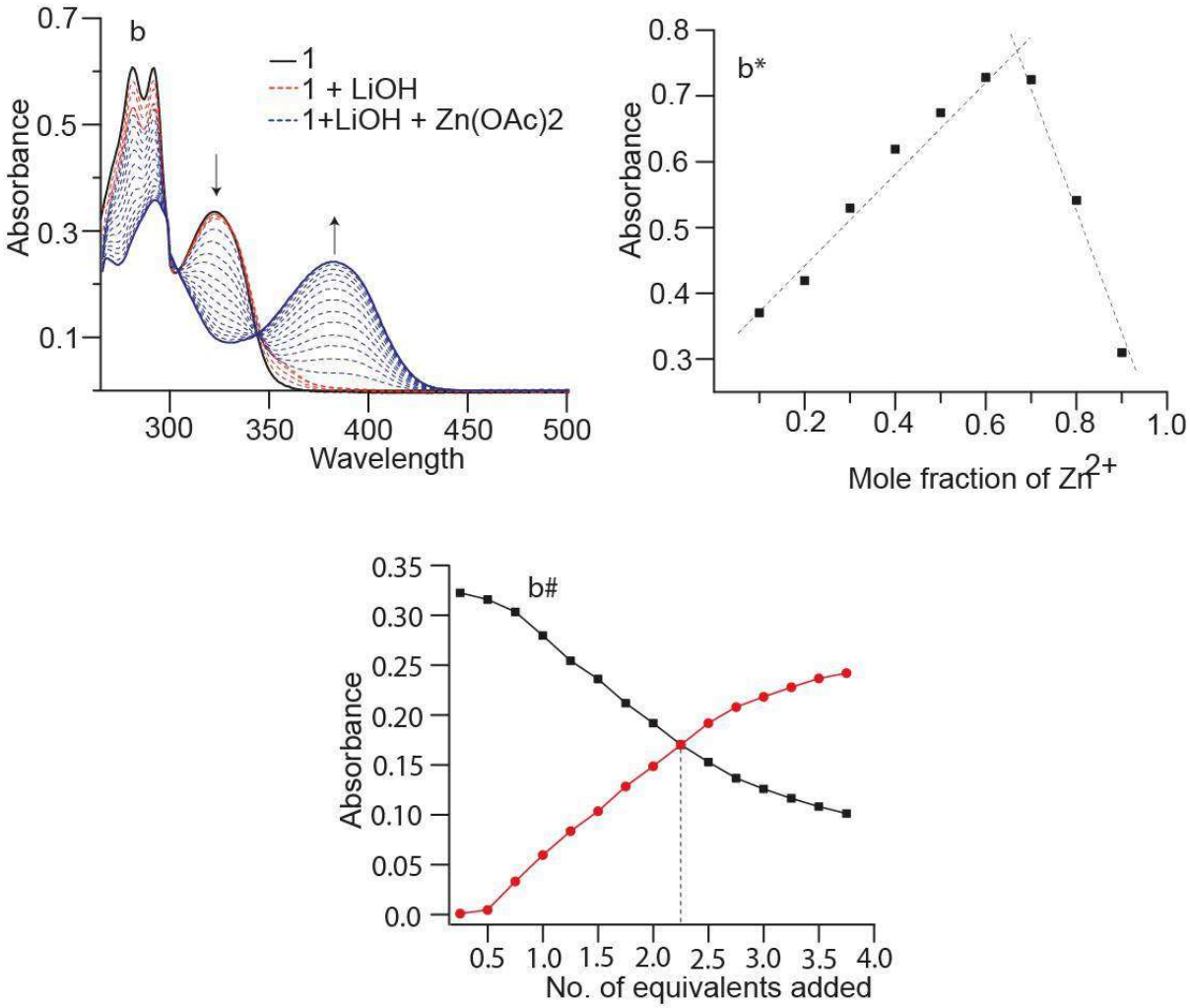

Figure 3.13 (b) UV-vis titration of Isomer 1 with $Zn(OAc)_2$ in the presence of LiOH as base showing nice isosbestic curves (b*) Job's Plot data of $Zn(OAc)_2$ with Isomer 1 ($b^{\#}$) Number of equivalents added till the last aliquot of metal addition

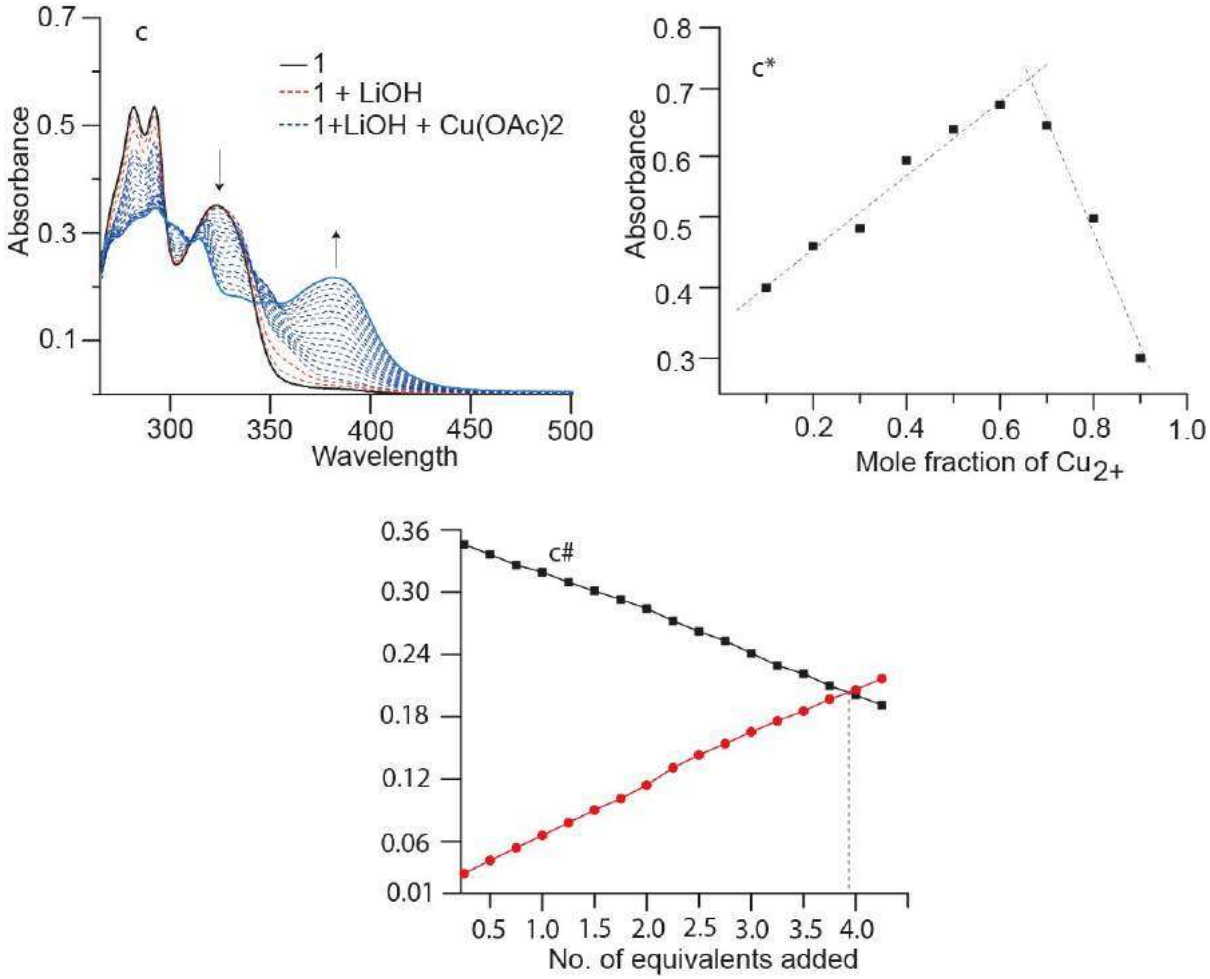

Figure 3.14 (c) UV-vis titration of Isomer 1 with $Cu(OAc)_2$ in the presence of LiOH as base showing dissimilar pattern from Cd(II) and Zn(II) (c*) Job's Plot data of $Cu(OAc)_2$ with Isomer 1 ($C^{\#}$) Number of equivalents added till the last aliquot of metal addition

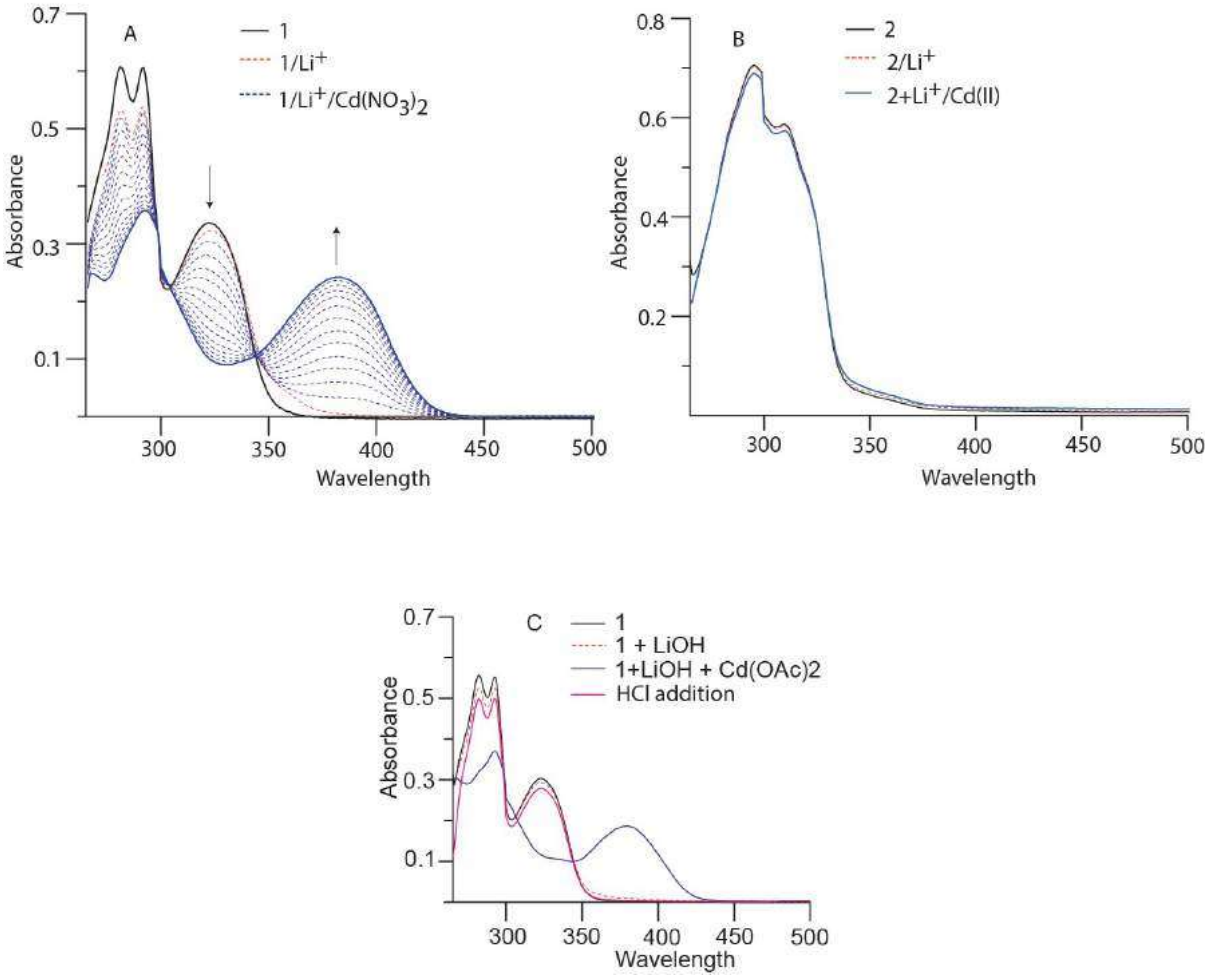

Figure 3.15 UV-vis titrations in DMF (A) ligand 1 (black line; λ_{max} 322 nm; $1x10^{-5}$ M), deprotonation with LiOH (3 equiv., red line) and upon aliquot addition of $Cd(NO_3)_2$ (blue line) band corresponding to ligand diminishes and a new band appears at 378 nm, simultaneously through isosbestic point; (B) similar titration experiment with isomer 2 in the presence of LiOH and $Cd(OAc)_2$, (C) Breaking of aggregation upon addition of HCl

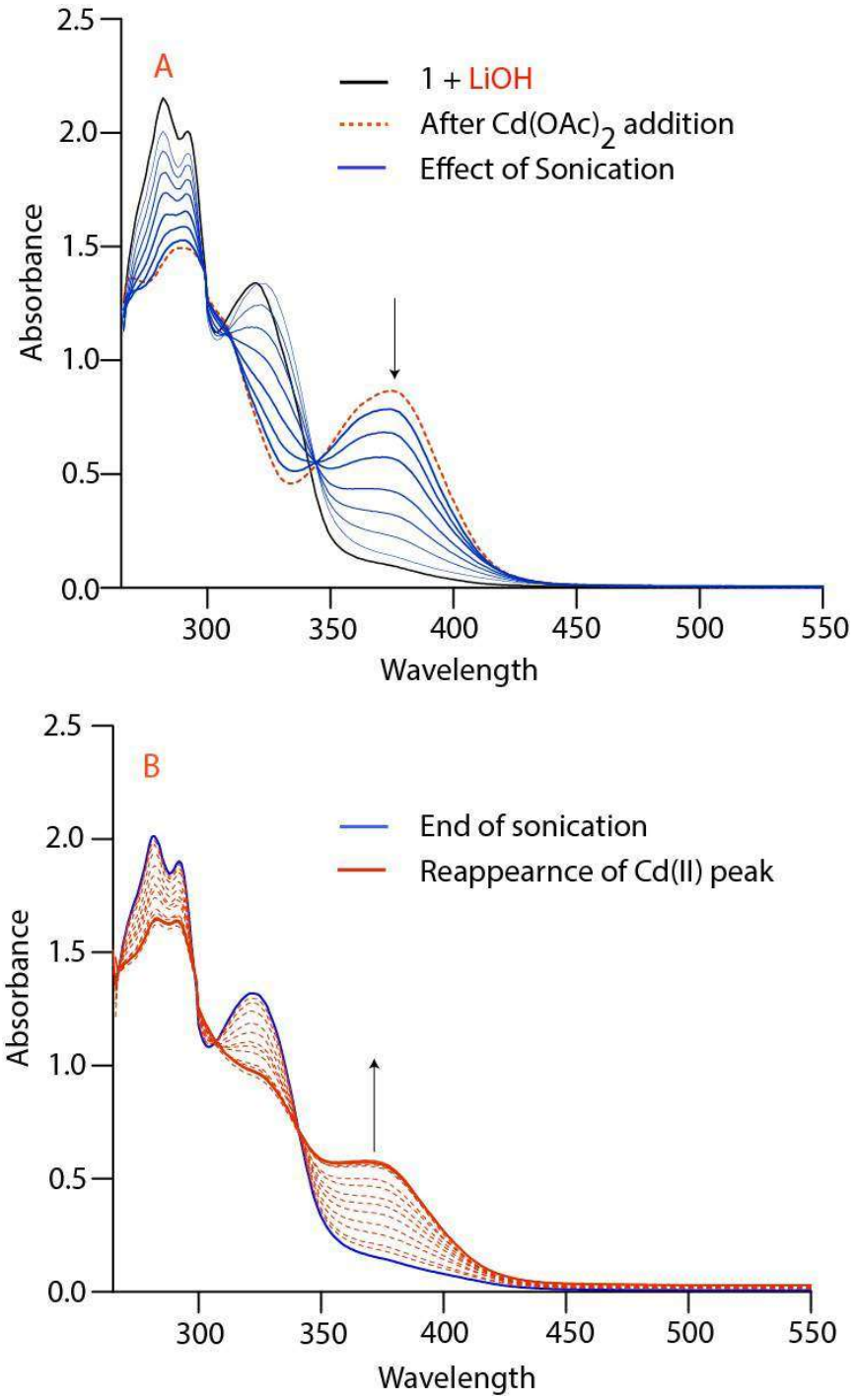

Figure 3.16 Effect of sonication monitored in UV-vis experiment of deprotonated 1 (0.5 x 10^{-4} M, DMF) (A) Band corresponding to 1/LiOH/$Cd(OAc)_2$ decreases and dynamically converted into band corresponding to ligand 1 upon brief sonication with 30 seconds interval suggests that there must be demetallation; (B) Again recover the band corresponding to Cd(II)-complex with resting time approximately 5 minutes

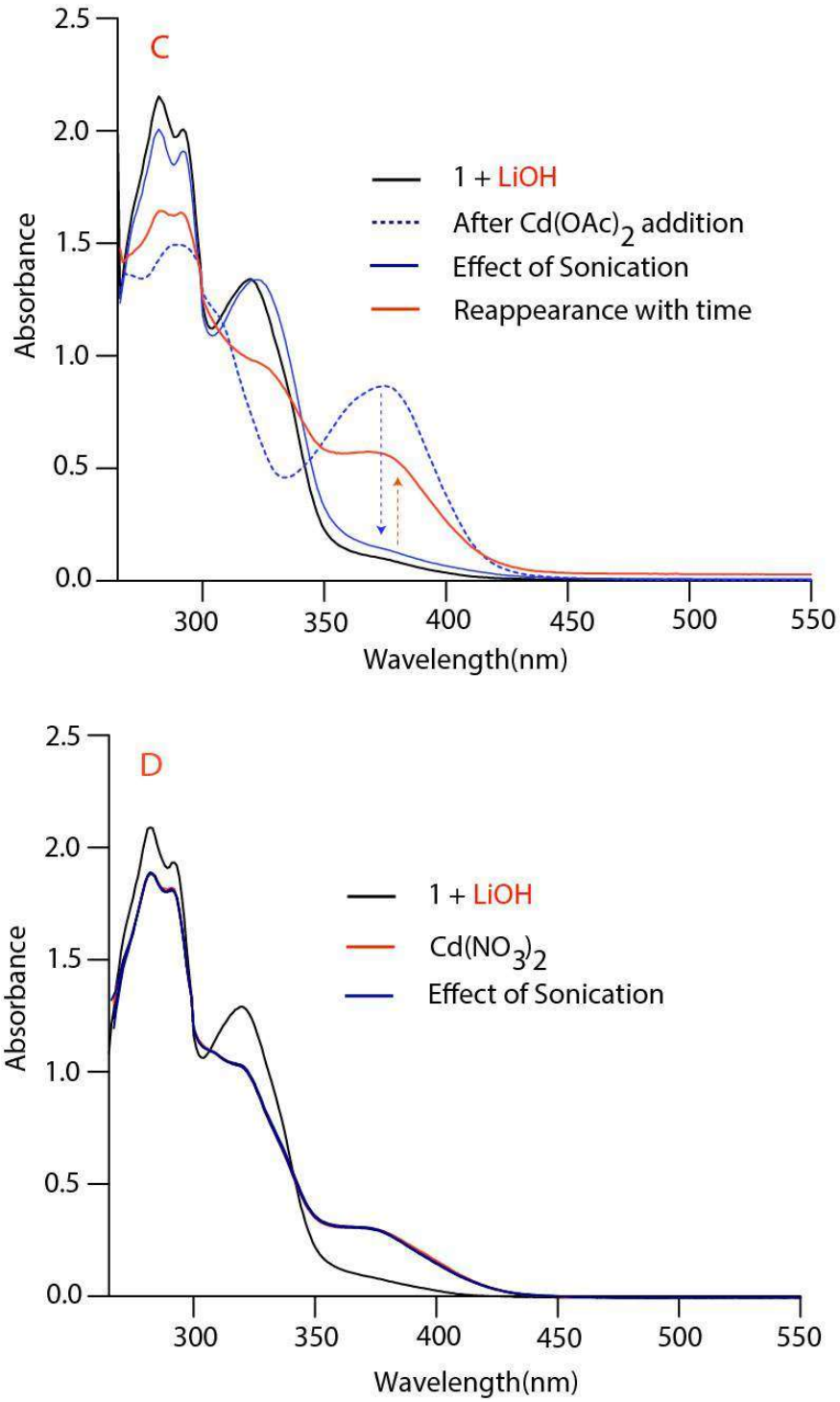

Figure 3.17 (C) Comparative decrease in absorbance with sonication and reappearance of peak with time indicates the demetallation with sonication and remetallation with resting, while (D) shows no effect of sonication with non-gelling combinations 1/KOH/Cd(OAc)$_2$ indicates role of Li^+ in gelation

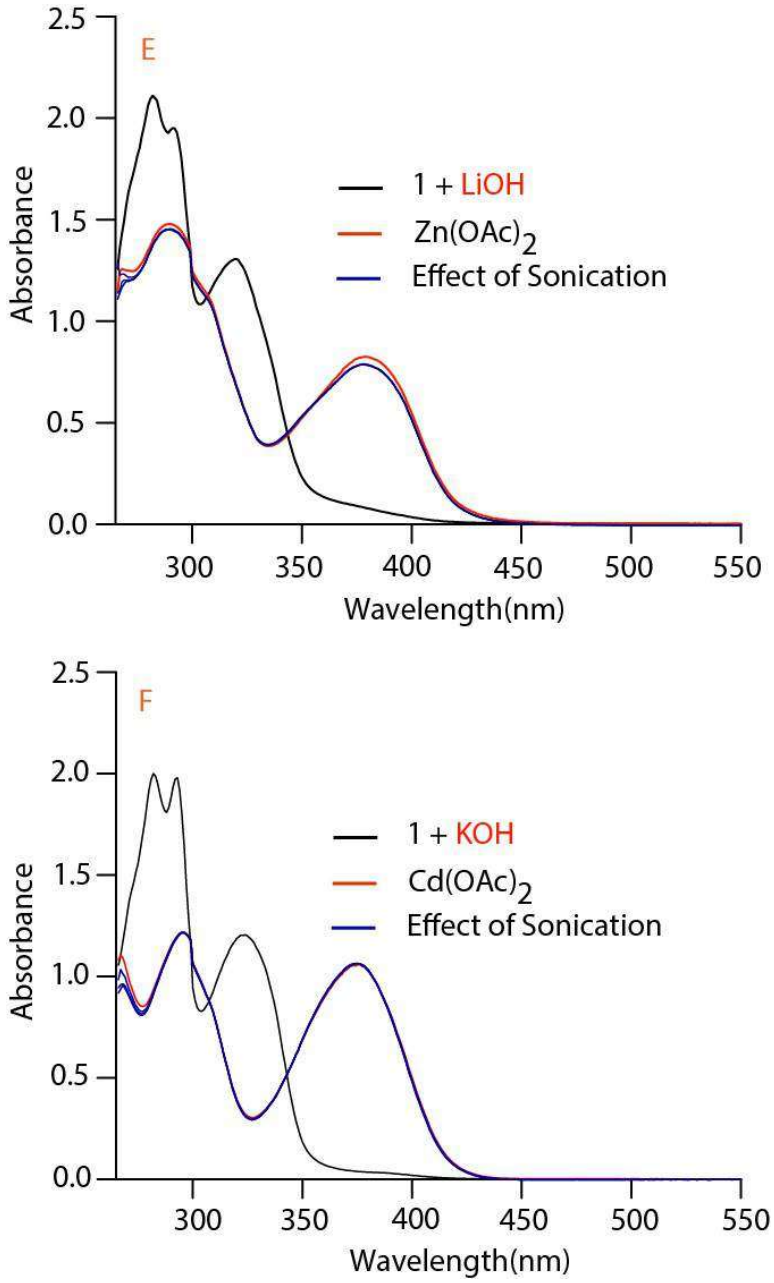

Figure 3.18 (E) shows no effect of sonication with non-gelling combinations 1/LiOH/$Zn(OAc)_2$ indicates the role of Cd^{2+} in gelation. (F) Shows no effect of sonication with non-gelling combinations 1/KOH/$Cd(OAc)_2$ indicates the role of Li^+ in gelation

3.4.10 Emission studies

The role of sonication in the aggregation process leading to gelation has been further investigated by fluorescence spectroscopy. The solution of 1 displayed a weak emission signal at 450 nm (1 x 10^{-4} M, DMF, λ_{ex} = 322 nm). The addition of LiOH led to a significant emission enhancement with a notable redshift of 45 nm (Stokes shift of 173 nm) (figure 3.19 A). The emission of 1/LiOH in DMF observed at 495 nm was then blue-shifted up to 468 nm ($\Delta\lambda$= 27 nm, Stokes shift= 146 nm) with substantial intensity enhancement upon complexation with Cd(II), as expected from chelation-enhanced fluorescence effects (CHEF). The most striking result was obtained under sonication conditions (figure 3.19 B). We found that sonicating a 1/3/1 mixture of 1/LiOH/Cd(II) in DMF for 1 min leads to a ~90% quenching of the fluorescence intensity coming along with a 8 nm blue shift of the emission signal (2x10^{-2} M, DMF, λ_{ex} = 378 nm, λ_{em} = 460 nm). Here again, these changes are compatible with a sonication-induced demetallation of the initial Cd(II) complex.

Further support for this statement was provided upon monitoring the changes in the fluorescence signature of the above sample once sonication has been turned off. These new conditions have indeed been found to result in a progressive enhancement of the emission signal coming along with a slight red shift of the emission wavelength of about 5 nm attributed to the cumulative effects of Cd(II) remetallation (CHEF) and of aggregation induced emission (AIE) (figure 3.22 C). The net quenching of about ~55% of the fluorescence intensity observed in the complete sonication-induced gelation process can be attributed to aggregation caused quenching (ACQ) [Ma *et al.* (2015)]. The presence of both the phenomenon of AIE (~45%) and ACQ (~55%) in gel making process was further

supported by the destruction of gel by dilution (0.6% w/v) experiment (figure 3.20). Two sets of changes were observed with the dilution of gel viz. fluorescence quenching in the range of 10^{-2} to 10^{-3} M and enhancement for 10^{-3} to 10^{-4} M dilution. These two sets of changes in terms of quenching and enhancement with dilution of gel prove the presence of both the AIE and ACQ in sonometallogel (figure 3.20). Thus, the sonication played key role in establishment of quite complicated phenomenon 'demetallation-remetallation-AIE-ACQ' in gel formation. To put more emphasis on the role of the sonication, aggregation and gelation processes, similar analyses have been conducted on non-gelling combinations like 1/LiOH/$Zn(OAc)_2$, 1/LiOH/$Cd(NO_3)_2$ and 1/KOH/$Cd(OAc)_2$, which differ in terms of the alkali base, anion or metal cation involved, respectively. For all these combinations, there was no significant change in the emission properties induced by sonication. Notably, a mixture of 1 and $Cd(OAc)_2$ displayed no change in emission during sonication, whereas further addition of the requisite amount of LiOH led to the expected quenching of the emission signal signifies role of LiOH in gelation. The weak emission of isomer 2 remained constant upon addition of LiOH, Cd(II) and upon sonication under similar conditions used for isomer 1, probably on account of the absence of chelation site and CHEF.

A comparative study of the average fluorescence lifetime estimated before and after sonication of gelling (1:LiOH:$Cd(OAc)_2$ τ = 1.023 and 0.556 ns) and non gelling (1:LiOH:$Zn(OAc)_2$; τ = 0.897 and 0.855 ns) combinations attests the aforesaid observations about the role of sonication in gelation, vide supra (figure 3.23).

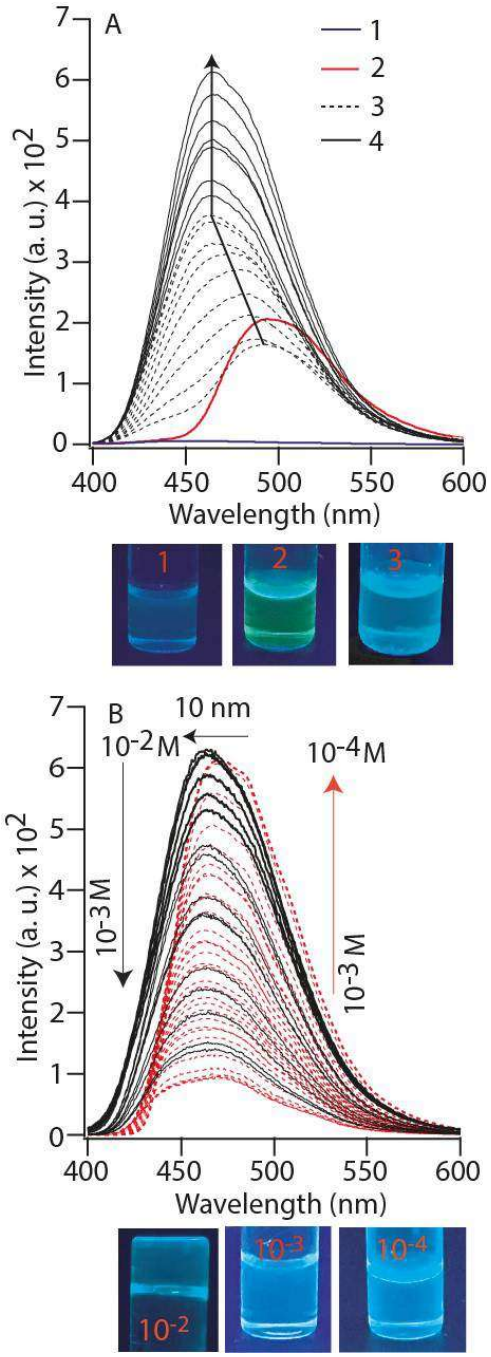

Figure 3.19 Fluorescence experiments in DMF (A) stepwise complex formation of isomer 1 (λ_{ex} = 322 nm, blue line, 1x10^{-4} M) with LiOH (red line) and Cd(OAc)$_2$ (black lines). (B) Effect of sonication (black lines, 2x10^{-2} M, 298 K) on the solution of 1/LiOH/(Cd(OAc)$_2$ and time-dependent evolution (black dotted and red lines)

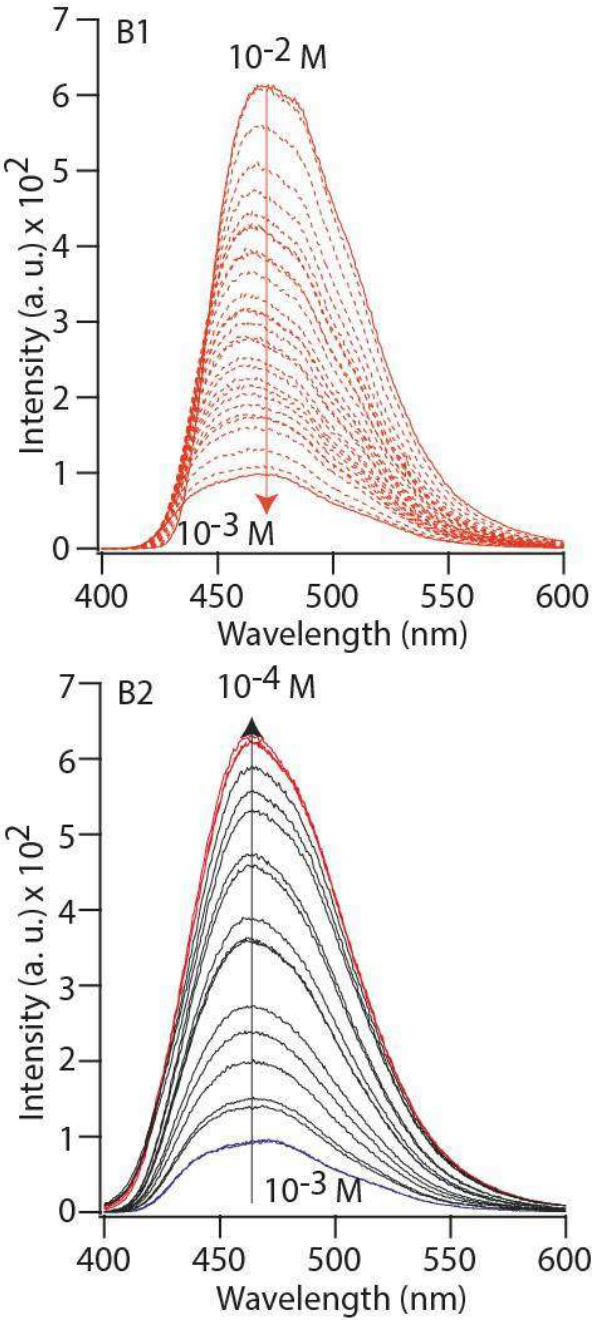

Figure 3.20 Fluorescence experiment (B1) and (B2), dilution of sonometallogel to prove the presence of AIE and ACQ phenomenon

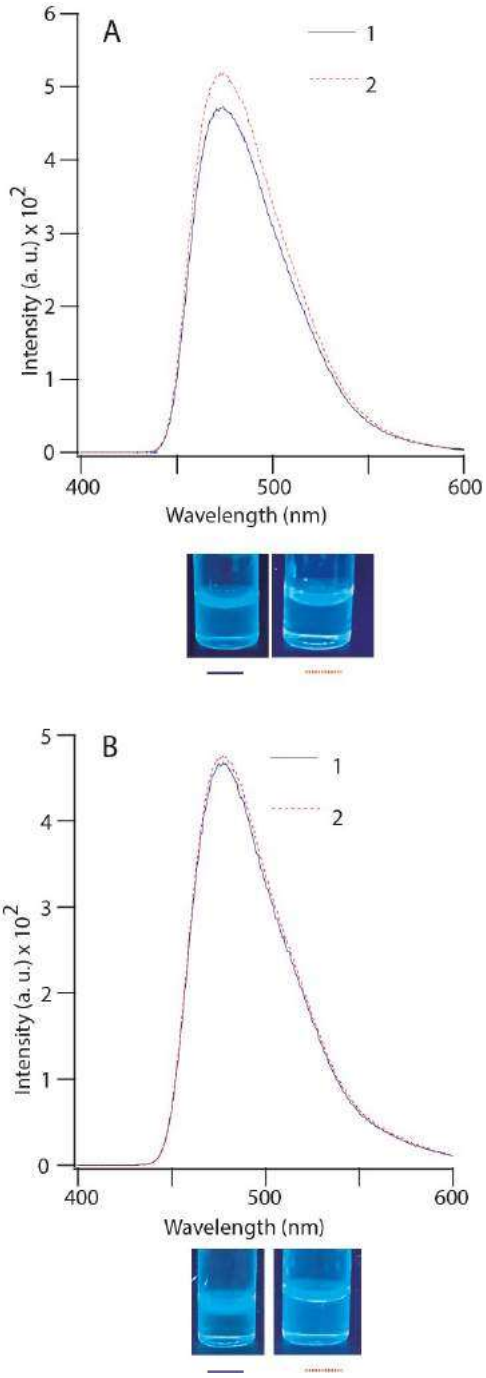

Figure 3.21 (A) Effect of sonication on flourescence spectra ($2x10^{-2}$ M, gelation concentration), where, blue line before sonication and red dotted line after sonication (B) There is no effect of sonication on the emission intensity of non-gelling combinations

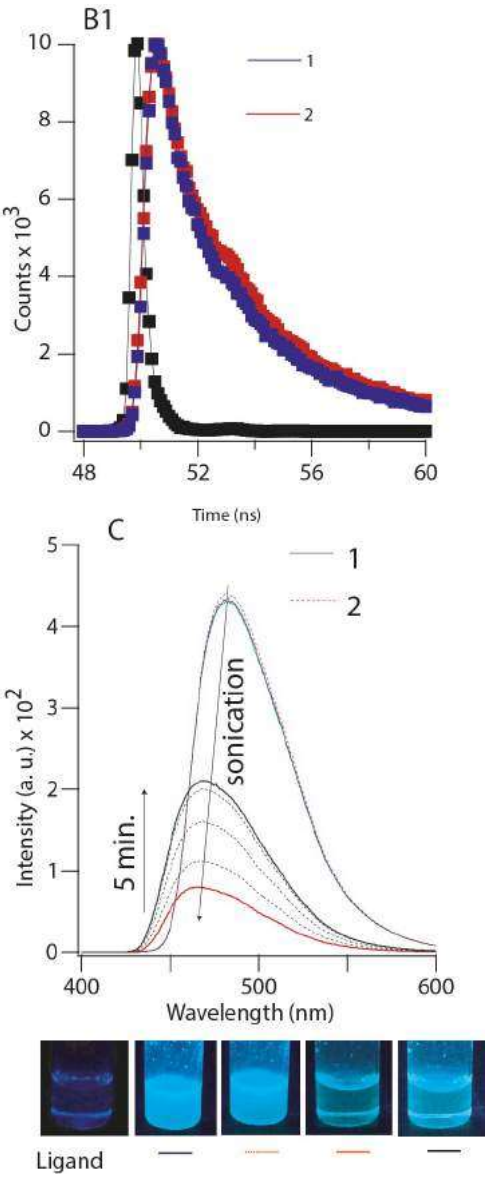

Figure 3.22 (B1) lifetime measurement corresponding to non-gelling combination 1/LiOH/$Zn(OAc)_2$, (C) The solution of 1/$Cd(OAc)_2$ before (blue line) and after (red dotted line) sonication, addition of LiOH and sonication (red continuous line) and increment in intensity with time (black lines)

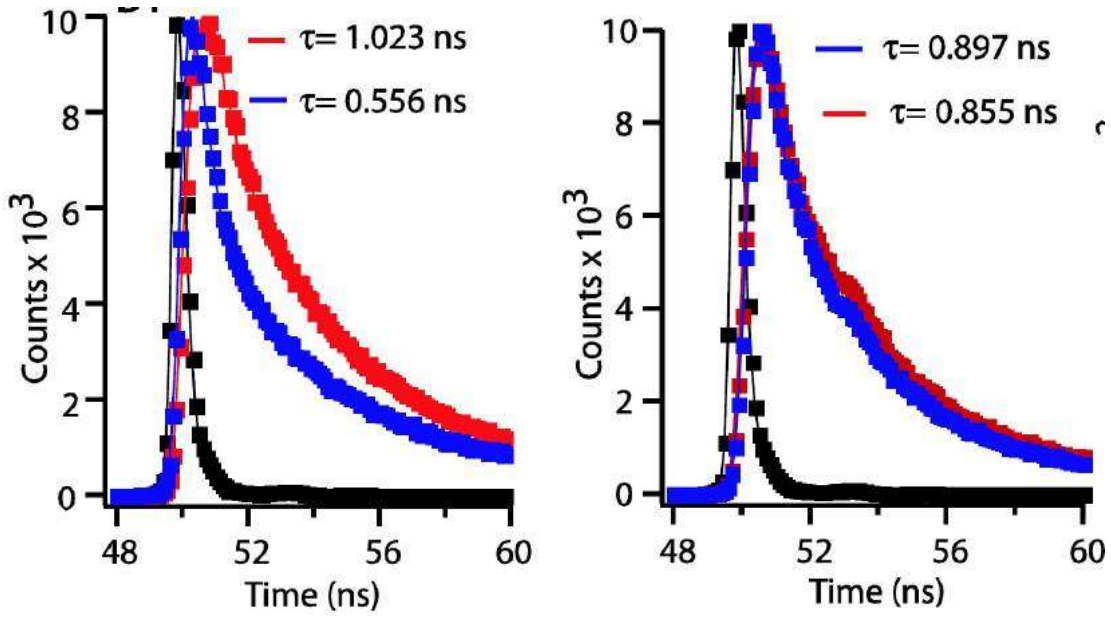

Figure 3.23 (left) Fluorescence lifetime measurement of 1/LiOH/$(Cd(OAc)_2$ before (red line) and after (blue line) sonication. (right) lifetime measurement corresponding to the non-gelling combination

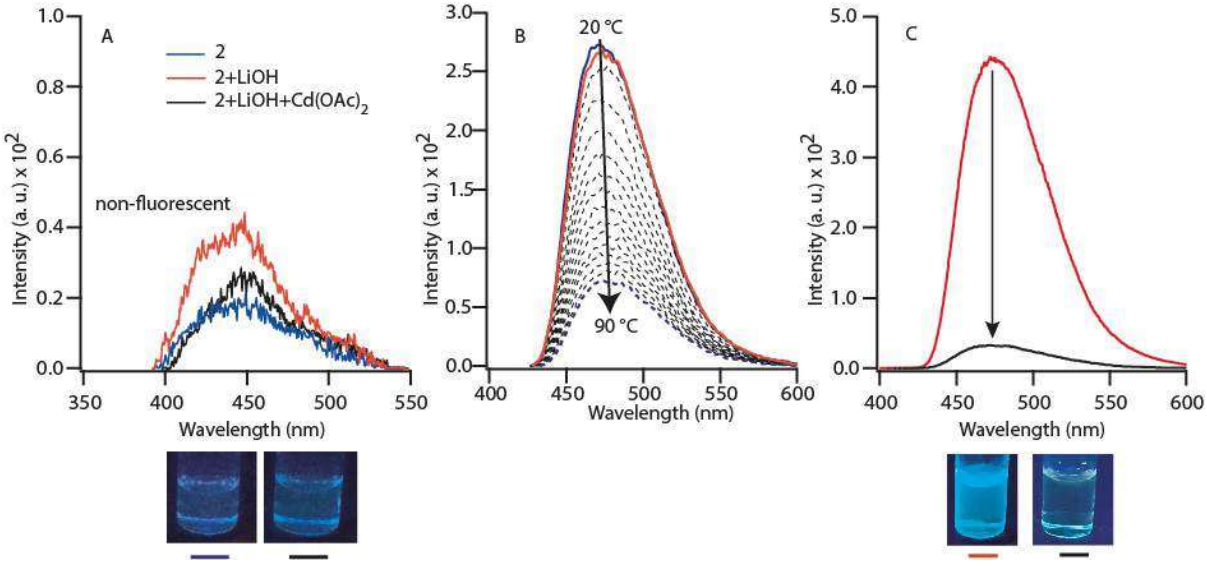

Figure 3.24 Fluorescence experiments in DMF (A) isomer 2 (λ_{ex} = 322 nm, blue line, $1x10^{-4}$ M) with LiOH (red line) and $Cd(OAc)_2$ (black lines) showing no major fluorescence. (B) Variable temperature in the range 20-90 °C of freshly prepared gel (0.6% w/v; λ_{ex} = 378 nm, blue line) and after cooling down to 20 °C (pink line). (C) Sonometallogel (red line, $2x10^{-2}$ M, λ_{ex} = 378 nm) after dilute acid treatment (black line) along with their visual changes

3.4.11 Structural Changes in Isomer 1 upon metal addition

All the possible conformations of 1 have been derived from IR, ^{1}H NMR, UV-vis and fluorescence (A) IR spectrum of isomer 1 shows characteristic bands at 3405, 1661-1621 and 1526 cm^{-1} corresponding to υ(OH), υ(C=O), υ(C=N), respectively; (B) Upon addition of Li^{+}, there is no significant change observed in peaks respective to C=O, but disappearance of band corresponding to υ(OH) along with slight shifting in υ(C=N) band to 1537 cm^{-1} suggests deprotonation and weak interaction of Li^{+} with C=N; (C) Addition of Cd^{2+} originate the shift in bands corresponding to υ(C=O) and υ(C=N) up to 1610, 1539 and 1470 cm^{-1} respectively along with a small un-shifted band corresponding to υ(C=O) at 1661 cm^{-1} suggests one C=O remains free from metal ion binding. Thus, it can be concluded that the eventual possible conformation is maybe syn-syn-anti conformer [Hosseini *et al.* (2014), Pandey *et al.* (2017)] (figure 3.25).

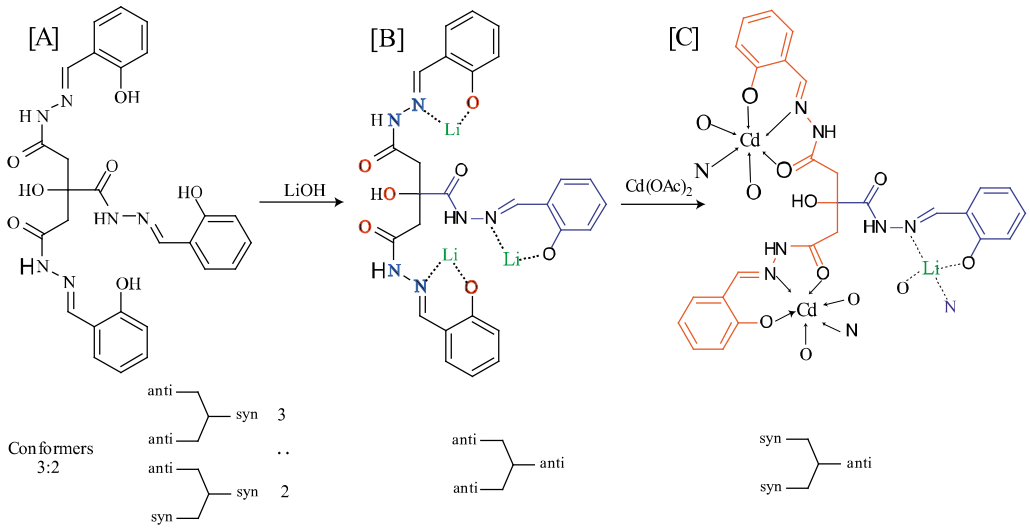

Figure 3.25 Sketch diagram shows the possibility of conformational changes in 1 at various stage (A) ligand 1 in two possible conformations anti-anti-syn and anti-syn-syn, (B) upon LiOH deprotonation (Li^+ interaction) of ligand changed into single conformation anti-anti-anti, (C) upon Cd^{2+} chelation again changes into syn-syn-anti conformation which has been justified by IR, UV-vis, fluorescence and NMR experiments

3.4.12 IR spectroscopy of Complexation

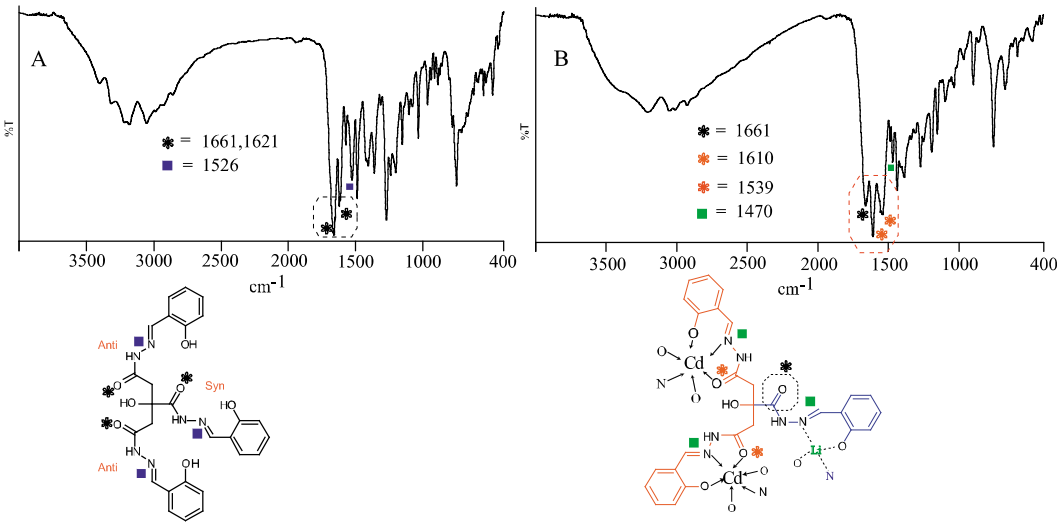

Figure 3.26 FTIR spectra for (A) Isomer 1 illustrate υC=O at 1661, 1621 cm^{-1} and C=N at 1526 cm^{-1}, (B) xerogel indicating the downshift of υC=O at 1610 and 1539 cm^{-1} and C=N at 1470 cm^{-1} along with unshifted peak related to C=O at 1661 cm^{-1}, which supports the binding mode of ligand with Cd(II) and Li^+

3.4.13 ESI-MS spectra of Isomer 1 and Metallogel along with complexation mode by Job's plot

The Job's method was used to demonstrate the 1: 1 stoichiometry of the complex formed in our experimental conditions between 1 and Cd(II). The latter was further confirmed by mass spectrometry data, the molecular ion peak observed on the spectrum recorded in ESI (positive mode) for diluted gels matching the isotopic abundance pattern at m/z = 659.08 (calcd. 659.08) corresponding to the $[1+Cd+H]^+$ species (figure 3.27 & 3.28).

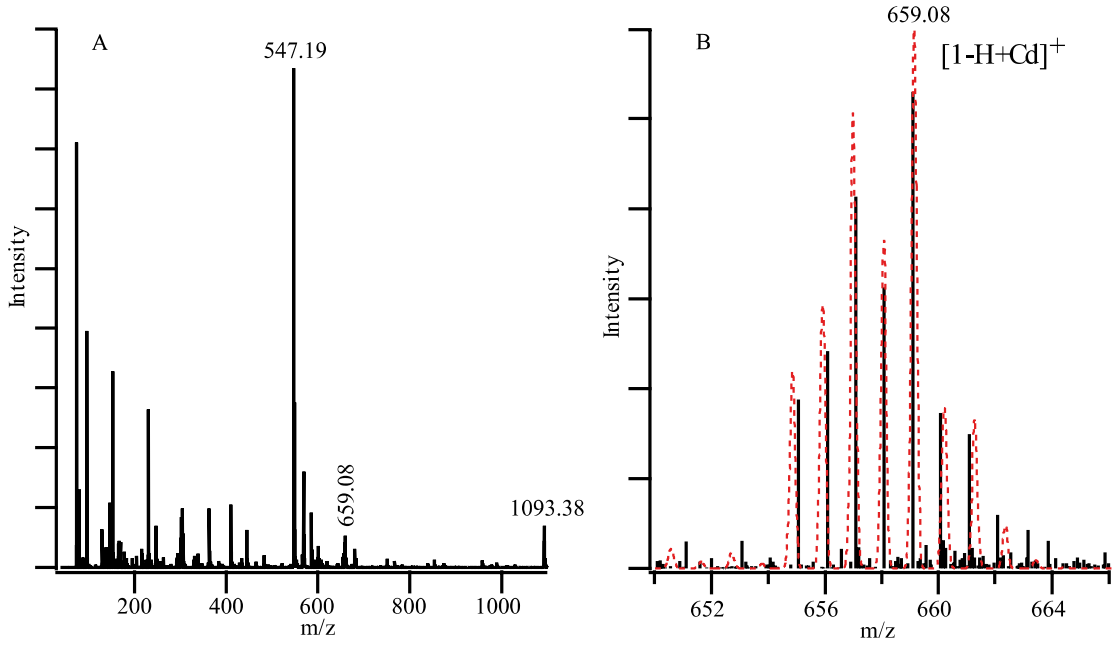

Figure 3.27 ESI-MS spectra of Isomer 1 and Metallogel where excellent corroboration with isotopic abundance pattern was observed in later

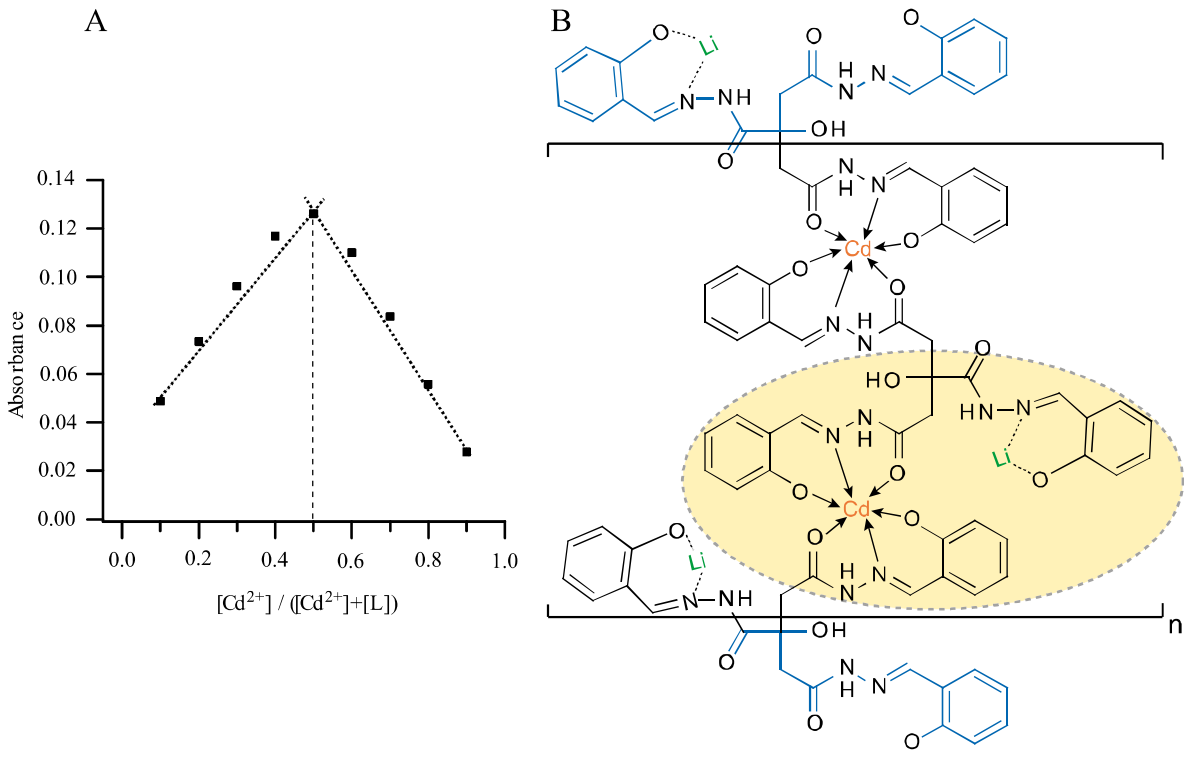

Figure 3.28 (A) Job's plot for LiOH deprotonated 1 vs. $Cd(OAc)_2$ showing 1:1 stoichiometry (B) The experimental isotopic abundance pattern of molecular ion peak of $[1+Cd(II)+H]^+$ matches nicely with simulated which supports the results obtained from Job's plot (C) The possible structure of complex is coordination polymer

3.4.14 Comparison of bonding mode for Isomer 1 in both combinations of metal

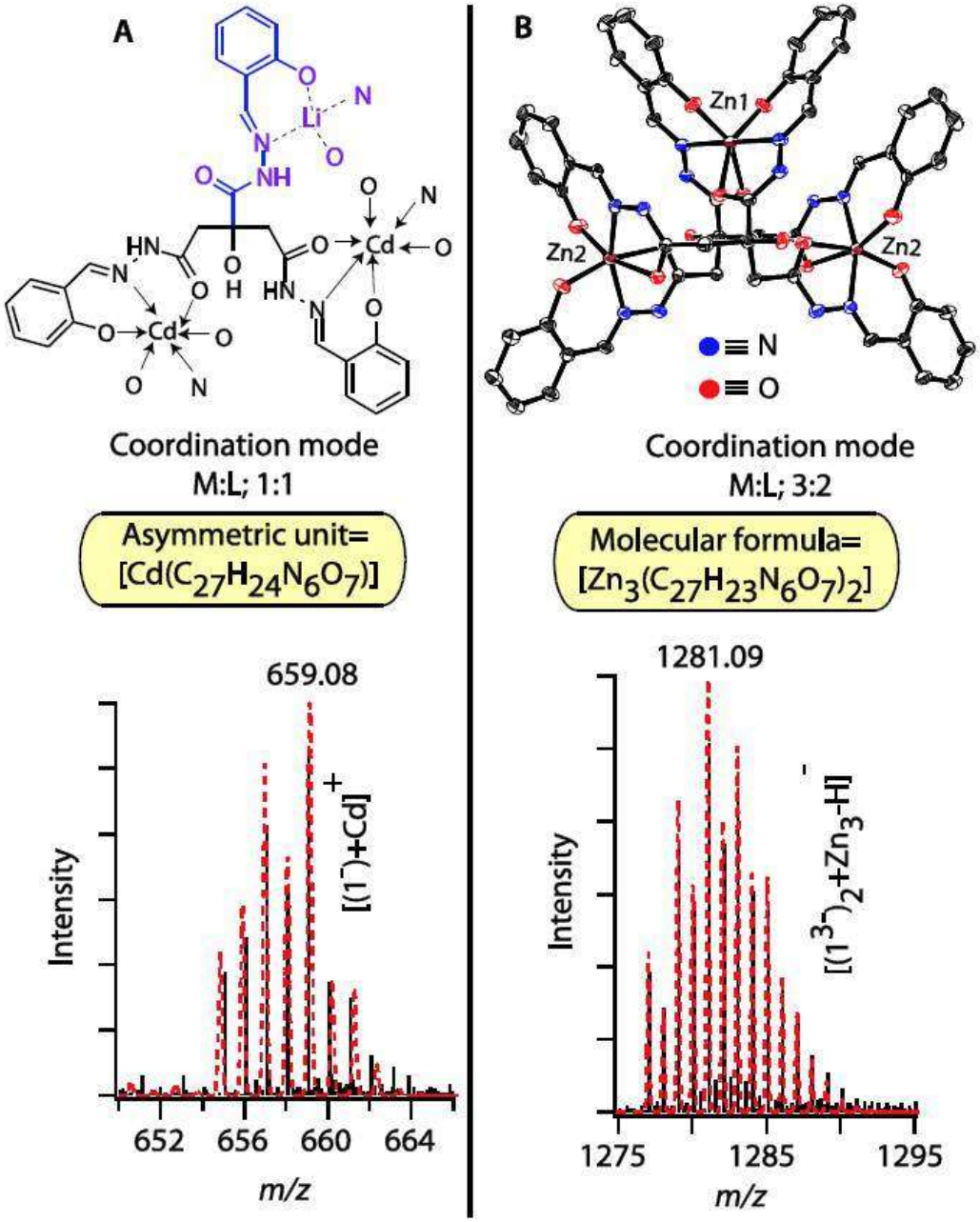

Figure 3.29 Sketch diagram of asymmetric unit (1/Li^+/Cd(II)) involved in sonometallogel formation along with isotopic abundance pattern of molecular ion (black line) matches nicely with simulated (red dotted) and (B) ORTEP diagram at 30% thermal ellipsoid probability of 1/Li^+/Zn(II) along with isotopic abundance pattern of molecular ion (black line) matches nicely with simulated (red dotted). The H-atoms are omitted for clarity

The structure of complex derived as coordination polymer demonstrated through sketch diagram along with the asymmetric unit highlighted through the colored circle. Crystal data: $C_{55}H_{90}N_{12}O_{38}Zn_3$, F_w 1723.50, T (K) 293(2), monoclinic, C2/c, a = 17.499(15) A°, b = 22.610(3) A°, c = 19.196(16) A°; β = 105.599, V=7316.0(3) A °^{3}, Z=4, F_{calcd}=1.565 Mgm^{-3}, μ=1.079 mm^{-1}, reflections collected 8013, independent 5197, R1=0.1025, wR2=0.2907 [I > 2σ(I)]; R1 = 0.1338, wR2 = 0.3597 (all data), GOF = 1.209. CCDC number 1524168.

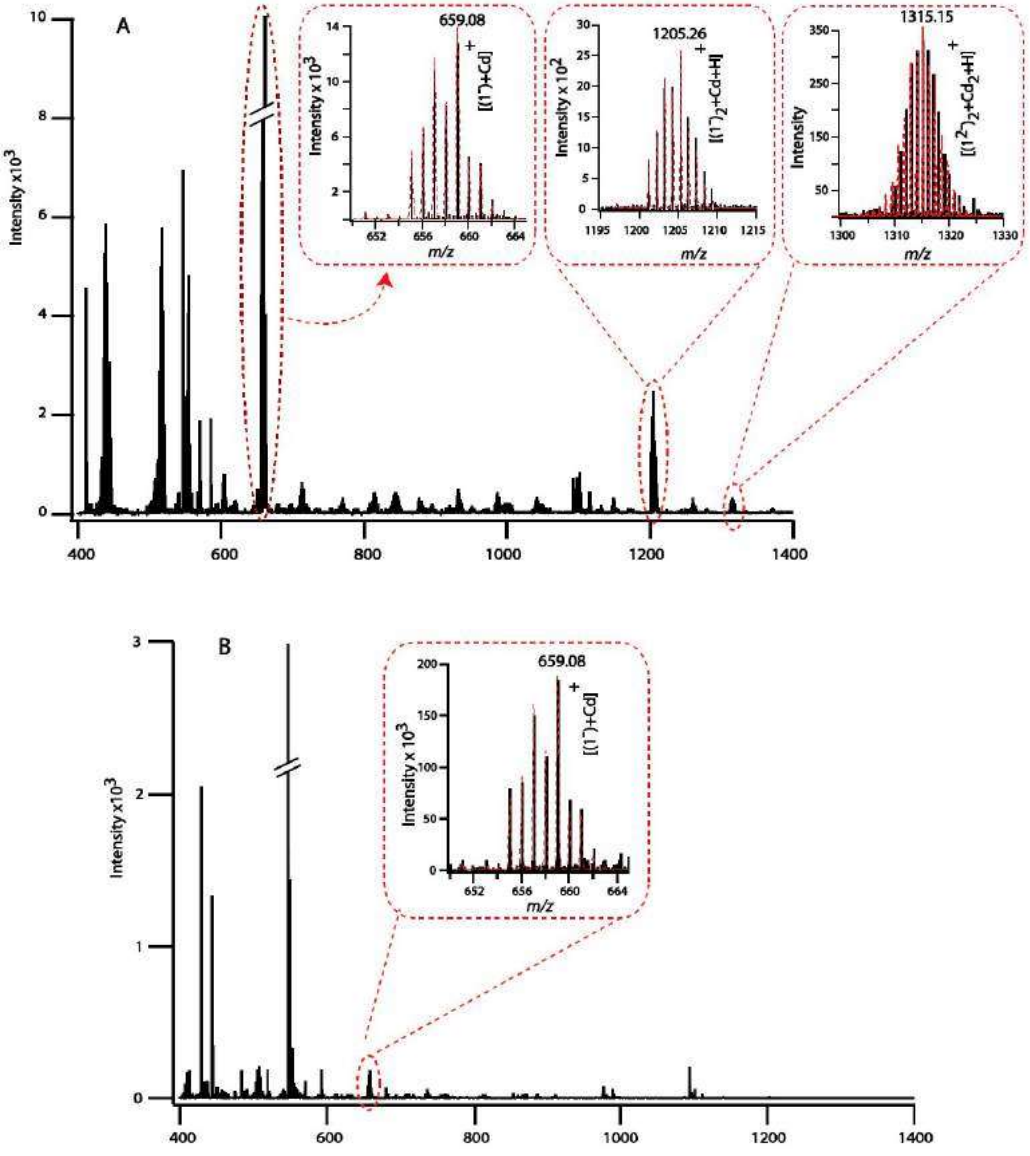

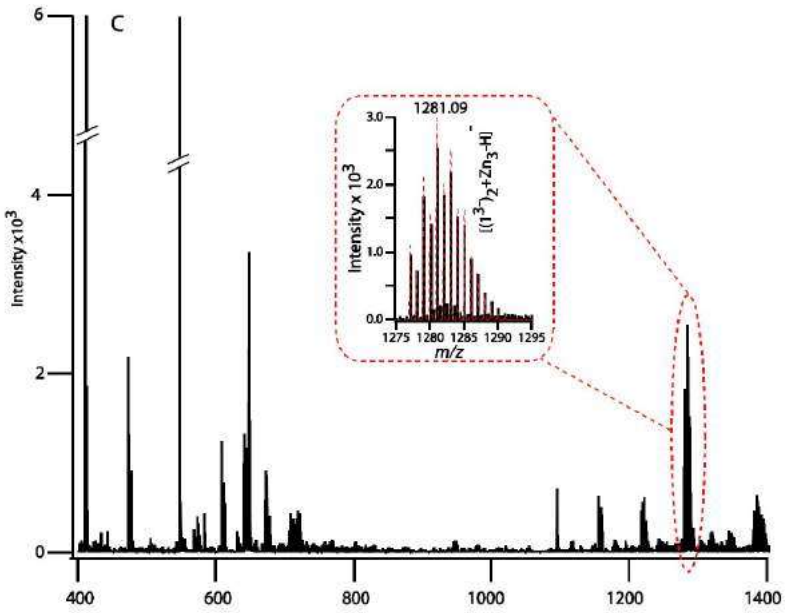

Figure 3.30 ESI-MS (DMF) spectra of (A) diluted metallogel shows the molecular ion peak of asymmetric unit m/z, [1+Cd(II)+H]$^+$, 659.08 (calcd. 659.08) with matching profile of isotopic abundance pattern of experimental (black line) and simulated (red dotted), supporting the complex formation is at 1:1 ratio. Further analysis of full-spectrum shows the repetition of asymmetric at m/z 1315.15 with the complete matching of isotopic abundance pattern of experimental (black line) with simulated (red dotted) confirms the coordination polymeric nature of structure involved in sonometallogel formation. (B) The mixture of 1/Li$^+$/Cd(II) before sonication exhibits very less intense asymmetric unit molecular ion peak at m/z, [1+Cd(II)+H]$^+$, 659.08 (calcd. 659.08), where isotopic abundance pattern of experimental matches nicely with simulated. Notably, other peaks are absent at higher m/z like 1315.15 which also confirms the role of sonication in stable coordination polymeric complex formation as well as gelation. (C) Crystals obtained from (1/Li$^+$/Zn(II)) combination shows the molecular ion peak at m/z 1281.09. The isotopic abundance pattern of experimental (black line) also matches nicely with simulated (red dotted line). Notably, there were no peaks observed for any indication of coordination polymeric complex formation which indirectly confirms the coordination polymer formation in sonometallogel

3.4.15 PXRD analysis of Metallogel, before and after sonication

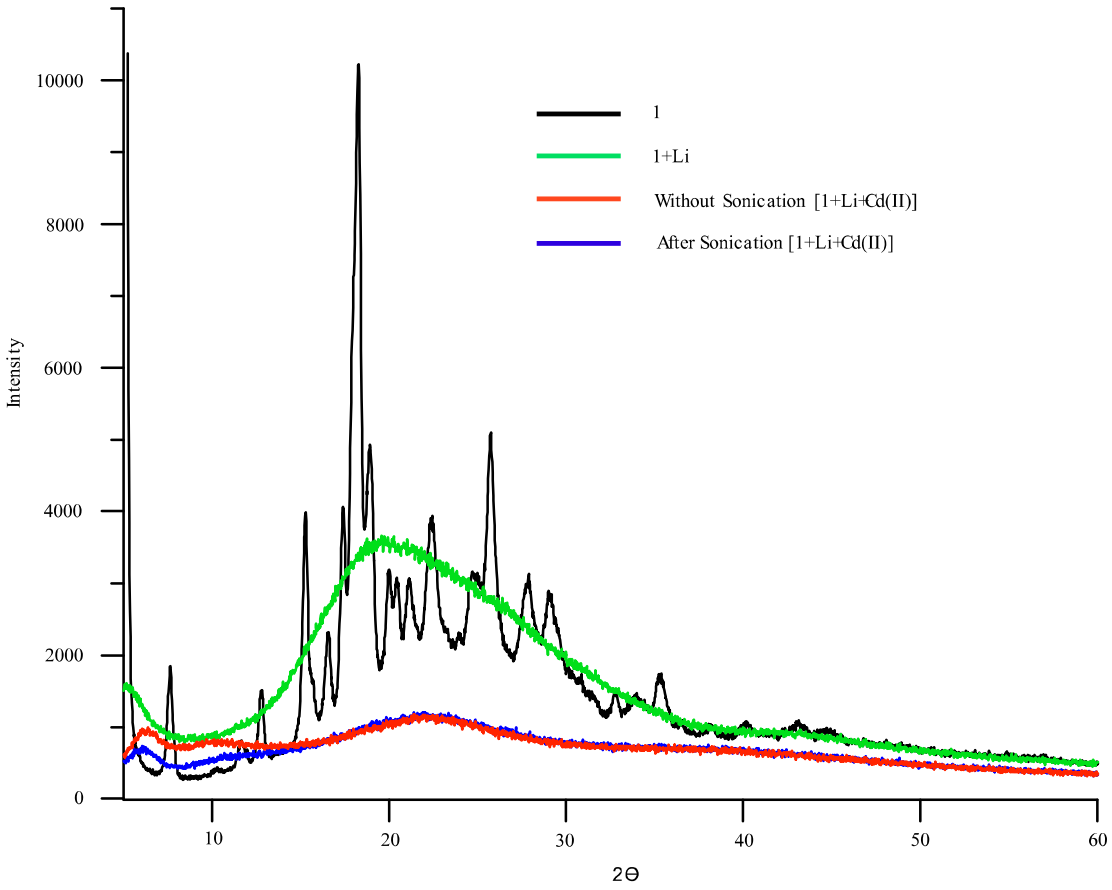

Figure 3.31 Powder X-ray diffraction pattern of isomer 1 (black line), 1/3 LiOH (green line), 1/3 LiOH/$Cd(OAc)_2$ (blue line; before sonication) and xerogel (red line) indicating ligand losses its crystalline nature upon deprotonation and completely amorphous upon complexation and gelation (xerogel)

3.4.16 Thermogravimetric analysis

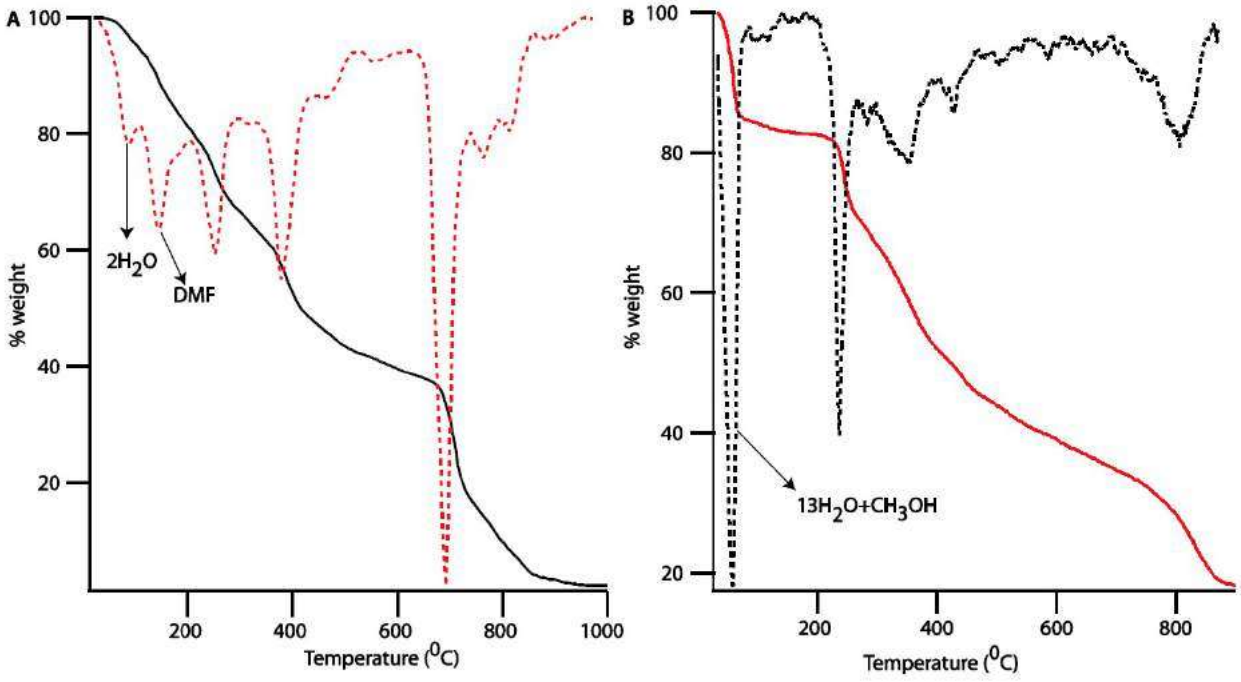

Figure 3.32 The Thermo Gravimetric Analysis (TGA) along with derivative plot for (A) the isolated compound from xerogel (washed with H_2O to remove extra salts and vacuum dried) shows 5.39% and 10.85% weight loss within the temperature range 45−190 °C, which suggests loss of two lattice water and one DMF molecules, respectively (weight loss as per TGA: 5.39% (calcd. for $2H_2O$ 5.47%); 10.85% (calcd. for DMF 11.09%) and 14.06, 13.75, 22.88% are corresponding to various kind of degradation of ligand) and (B) the crystals exhibits weight loss as per TGA: 15.66% (calcd. for: $13H_2O + CH_3OH$ 15.63%) which was also observed in crystal structure

3.4.17 Rheology

The viscoelastic behavior is typical of power-law gels with an elastic modulus G'≈2 kPa that remains one order of magnitude larger than the viscous modulus G"≈300 Pa and increases as a weak power law of frequency almost proportional to G". When the metallogel is submitted to oscillatory shear of increasing amplitude, it yields (G'≈G") at a critical strain y≈1.8%, which corresponds to a yield stress y≈20 Pa. For larger amplitudes, the system behaves as a liquid (G"≫G'). Such rheological data are fully consistent with the qualitative features of a solid gel that can easily be cut through, injected, and reversibly fluidized. Both moduli go through a broad maximum with the temperature at T≈80°C and the gel loses its solid-like properties, i.e., melts, for T_{gel} ~120°C. Such a high temperature for the gel-sol transition can be correlated with the boiling point of DMF (153 °C). It also supports the qualitative observation of thermoreversibility up to ~90 °C, above which the solid behavior is not recovered upon cooling. (Figure 3.33) Thus, quantitative rheological data confirm qualitative observations of the system gel properties [Jaishankar *et al.* (2014)].

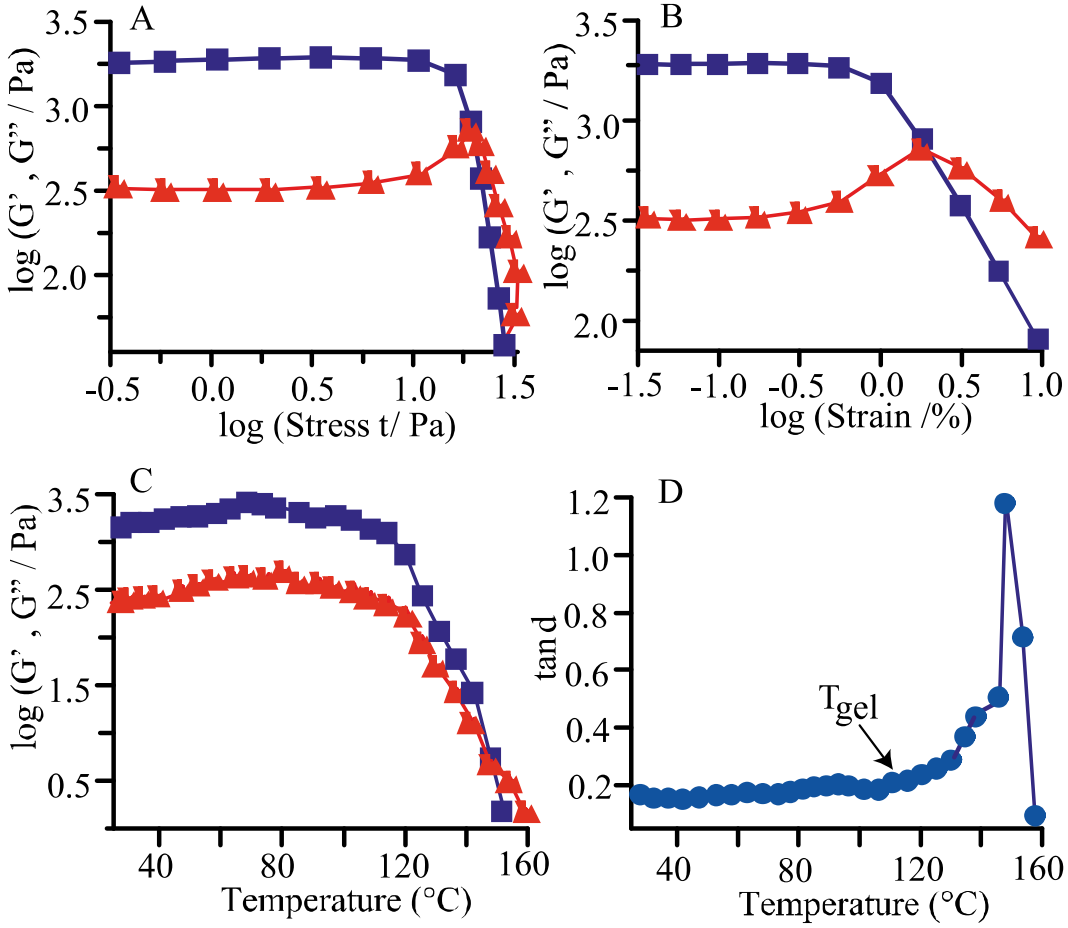

Figure 3.33 Rheology of the freshly prepared gel (0.6%, w/v) (A) Dynamic shear stress of Storage modulus (G′) and loss modulus (G″) at frequency of 0.01 rad s^{-1} and 25 °C, (B) Dynamic frequency sweep for G′ and G″ with the applied strain, (C) G′ and G″ in the temperature range 25 – 160 °C indicates the deformation of gel starts from ~110 °C and finished at ~150 °C and (D) The plot between loss tangent (tan δ) and temperature also suggests that the long range deformation of gel with a T_{gel} ~110°C

3.4.18 Conductance study

The impedance curve recorded in the same experimental condition after sonication shows a quite similar shape in the low frequency region with a straight line featuring a similar slope to the curve recorded before sonication. It reveals however that sonication results in a tenfold decrease of the measured resistance value from 15938 ohms down to 1724 ohms. This large drop of the resistance value comes along with the virtual disappearance of the semi-circular arc attributed to the cell capacitance whose characteristic frequency is now shifted to much higher, and thus hardly accessible, values. In this case, the electrolyte resistance R_1 could be obtained by extrapolation of the linear part of the curve up to its intersection with the real part of the impedance. Such unprecedented and spectacular effect, albeit still not fully understood, could potentially be explained by the improved mobility of charges carriers within the gel due to lesser solvation of ions or to a larger degree of dissociation of ion pairs. Another line of explanation to be considered is that the greater organization of molecules within the gel matrix could also have an effect on the diffusion of species towards and from the electrode. It has already been investigated that greater organized or ordered systems in terms of ions usually shows more conductance than randomly arranged systems. The conductivity of the gel was further investigated at different temperatures, between 293 and 338 K. As seen in the log k= f(1/T) curve shown in figure 3.34, the impedance response is found to be fully stable in that temperature range while significant drift starts to be observed only beyond 343K. (Figure 3.34) The stability of the response was further demonstrated upon showing that the resistance measured at 293 K can be recovered, with a drift lower than 4%, after heating the sample for more than 2 hours up to 343 K [Puigmartí-Luis *et al.* (2007), Dak *et al.* (2014), Hirschorn *et al.* (2010)].

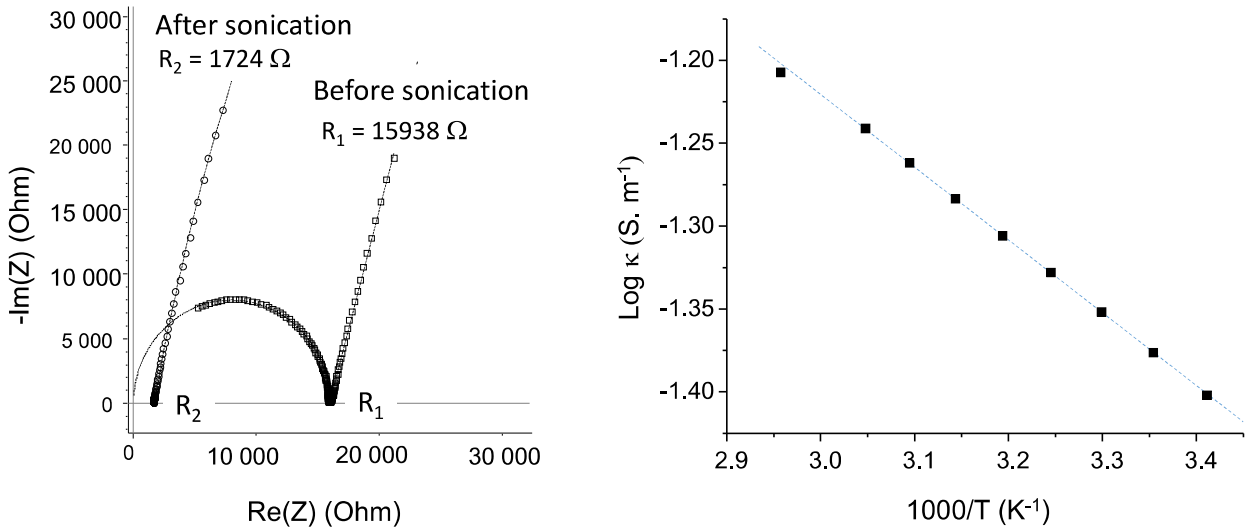

Figure 3.34 (Left) Experimental Nyquist impedance diagrams (–Im(Z) vs. Re(Z)) measured between 2.5 MHz and 1 Hz on the same sample at 291 K before and after a 2 min sonication step. Dotted lines represent the best fit model obtained with three components equivalent circuits R_1+Q_1/R_2 (after sonication) or C_1/R_1+Q_1 (before sonication). (Right) Temperature dependence of the ionic conductivity measured on the gel sample

3.4.19 NMR titration

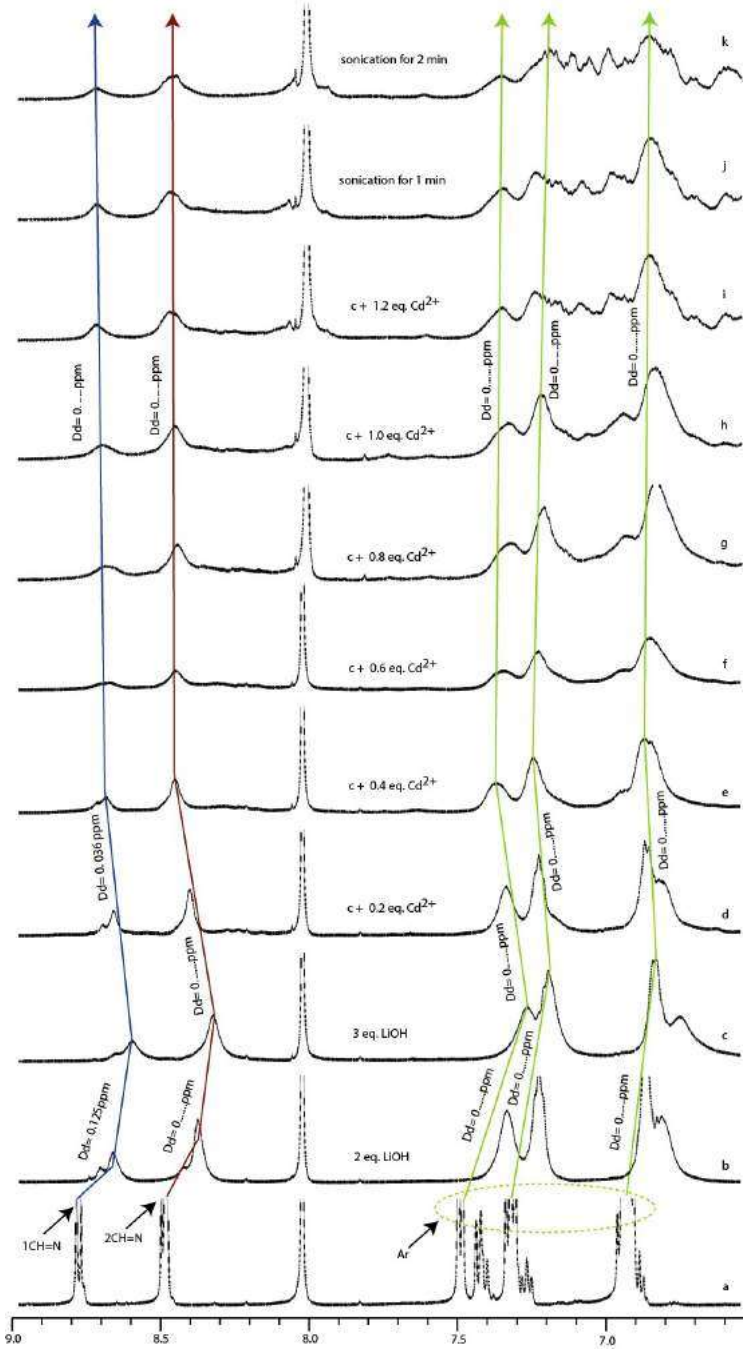

Figure 3.35 NMR titration of isomer 1 with LiOH and $Cd(OAc)_2$ exhibiting peak shift towards downfield upon LiOH addition which further retains back upfield upon addition of $Cd(OAc)_2$

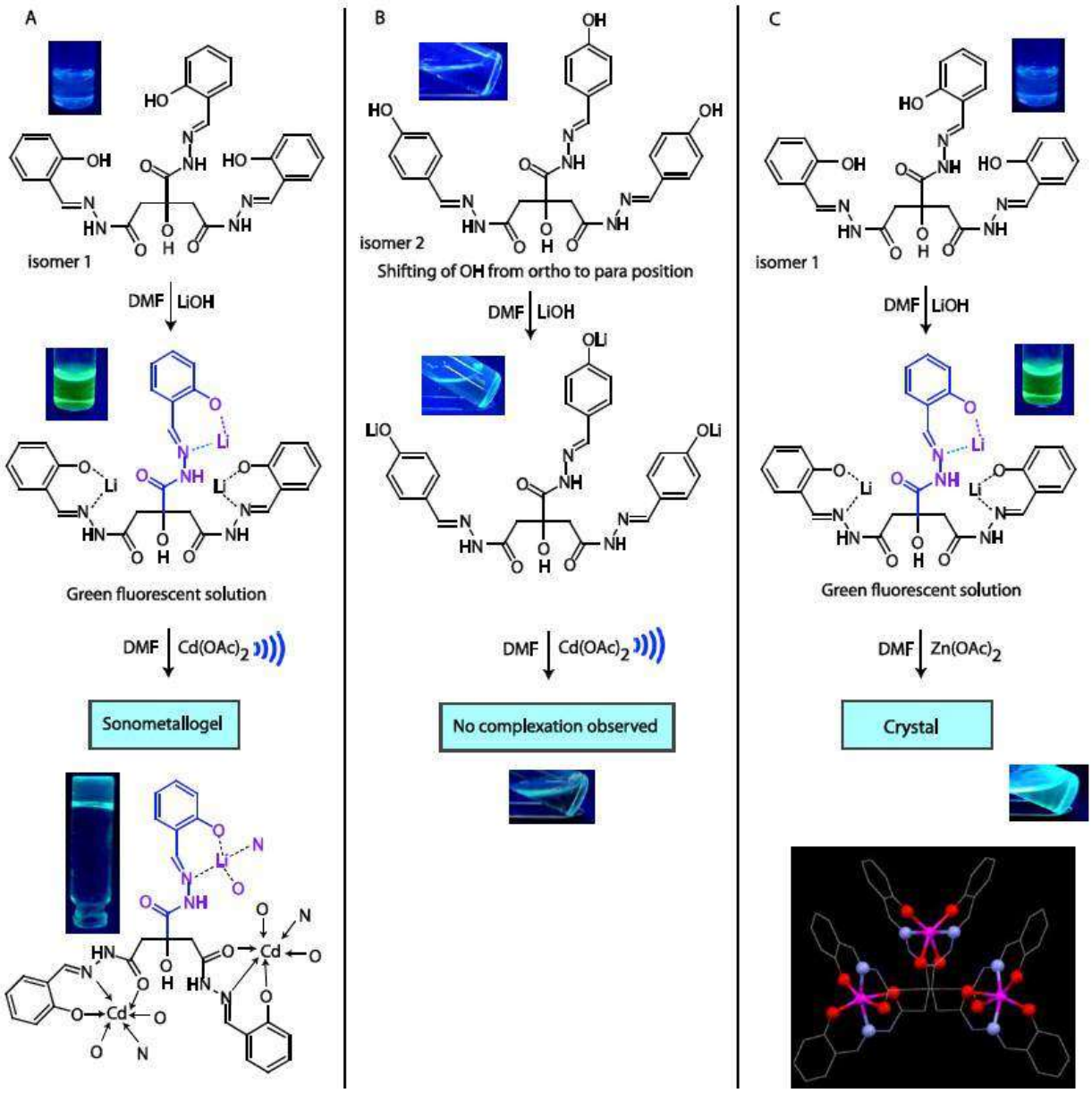

Figure 3.36 A comparative stepwise synthetic scheme along with fluorescence change (A) structural (positional) isomers 1 produce fluorescent metallogel upon reaction with LiOH and $Cd(OAc)_2$ in DMF under ultrasonication. The structure of metallogelator and xerogel could derive from various instrumental techniques. (B) regioisomer 2 produces non fluorescent solution under similar reaction conditions to isomer 1. (C) Isomer 1 produces fluorescent crystals when Cd(II) is replaced by Zn(II). The crystal structure and it's solution studies show the binding mode and ration of metal-ligand different from Cd(II)- gel structure, it is probably due to structural dissimilarity with Cd(II) and Zn(II) produces two different entity *viz.* gel and crystal

3.4.20 Mechanism of formation of metallogel

Isomer 1 undergoes conformational change towards the more stable anti-anti-anti structure in the presence of Li^{+}. Fluorescence enhanced upon Cd^{2+} addition to deprotonated 1, maybe due to chelation (CHEF). The TEM image at this stage shows the non-directional wrecked aggregate growth. Furthermore, upon brief sonication, de-metalation was evidenced by fluorescence and UV-vis spectroscopy. The fluorescent gel obtained within 5 min resting time. Gelation is due to remetalation/reorganization is well established by UV-vis and fluorescence studies. Based on results obtained from ESI-Mass, Job's plot, IR, TGA, molar conductance, we conclude that the final gel structure may be coordination polymer which further undergoes aggregation into nanofibers, facilitates the entrapment of solvent and eventually the fluorescent sonometallogel.

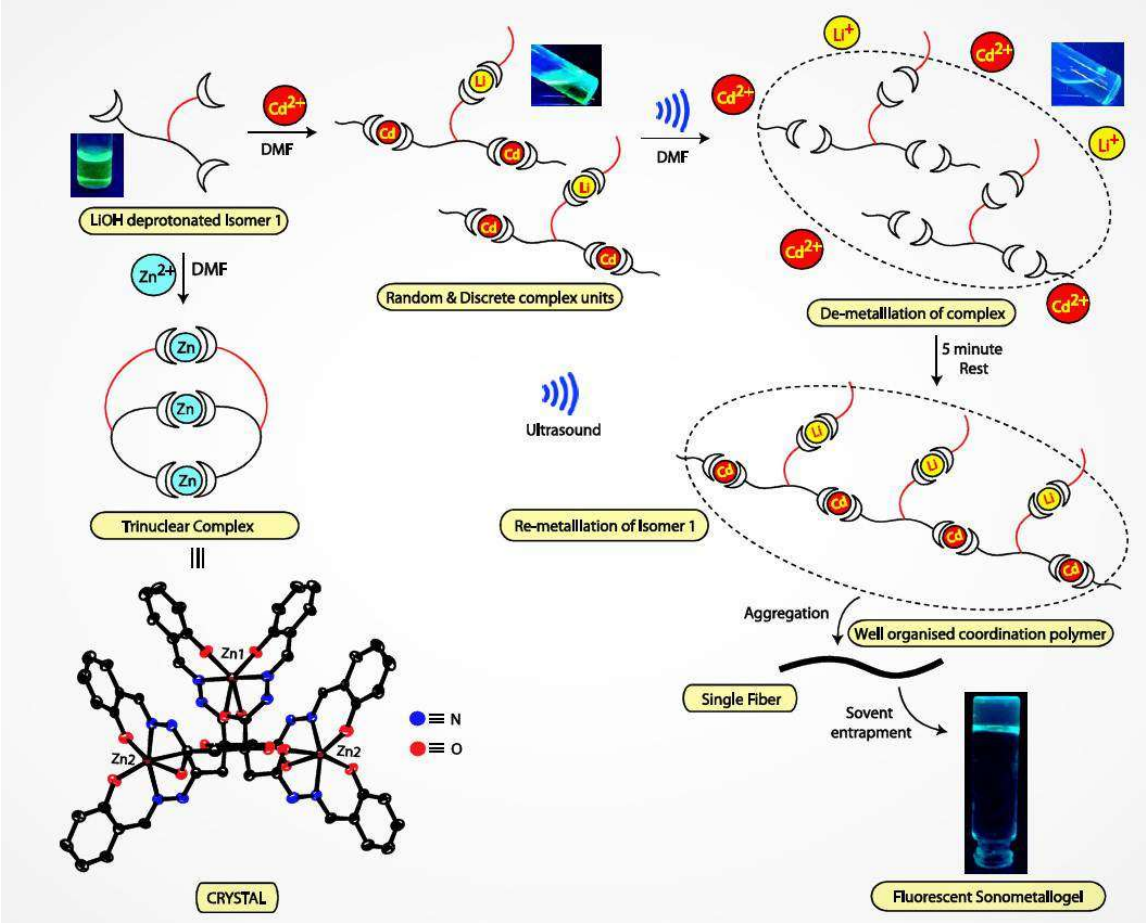

Figure 3.37 A model representation of plausible mechanism of the gelation along with structural changes under the influence of ultrasonication, while Zn(II) produces crystal structure. ORTEP diagram with 30% thermal ellipsoid probability and H atoms are removed for clarity

3.5 Conclusion

In conclusion, we have presented the synthesis and properties of an ultrasound-induced multi stimuli-responsive fluorescent sonometallogel produced from a highly selective combination of a non-fluorescent citric acid derived ligand, LiOH and $Cd(OAc)_2$ in DMF. Ultrasound not only promotes a series of demetallation-remetallation/reorganisation processes yielding Cd(II) adducts featuring outstanding gelation abilities; it also triggers the formation of well-defined cross-linked nanofibers bringing about an unprecedented enhancement of the conductivity. For the first time, we have established that a coordination complex undergoes gelation through demetallation followed by remetalation and necessary reorganization when subjected to ultrasound. The crystal structure obtained from $1/Li^+$/Zn (II) supports the different structures with $1/Li^+$/Cd (II) involved in gelation. In this regard, we anticipate that our inputs will provide new opportunities for the construction of efficient conductive sonometallogels.